THE GEOLOGICAL SOCIETY
OF AMERICA®

Geometry and magnitude of extension in the Basin and Range Province (39°N), Utah, Nevada, and California, USA: Constraints from a province-scale cross section

Sean P. Long[1,†]

[1]*School of the Environment, Washington State University, Pullman, Washington 99164, USA*

ABSTRACT

The Basin and Range Province is a classic locality of continental extension, and it is ideal for analyzing factors that control the collapse of thickened orogenic crust. However, the magnitude and distribution of extension, which are critical parameters for this analysis, remain poorly constrained in many areas. To address this problem, a cross section spanning the province at ~39°N is presented. Retrodeformation yields 230 ± 42 km of cumulative extension (46% ± 8%), and an average pre-extensional thickness of 54 ± 6 km. When viewed at the scale of multiple ranges, two high-magnitude (~60%–66%) and two low-magnitude (~11%) domains of extension are apparent, and each can be related spatially to portions of the Cordilleran orogen that have high and low predicted crustal thickness, respectively. The eastern high-magnitude domain restores to a 60 ± 11 km thickness and corresponds to the western portion of the Sevier thrust belt and the estimated spatial extent of thick, underthrusted North American crust. The western high-magnitude domain restores to a 66 ± 5 km thickness and corresponds to the eastern part of the Sierran magmatic arc. Thickness variations inherited from Cordilleran orogenesis are interpreted as the primary control on extensional strain distribution. The eastern domain underwent a protracted, Late Cretaceous–Miocene transition to an extensional regime, while widespread extension in the western domain did not start until the Miocene, which is attributed to upper-crustal rheological differences between the granitic arc and the sedimentary section in the retroarc. Most extension can be temporally related to geodynamic driving events, including delamination, slab rollback, and plate-boundary reorganization, which caused gravitational collapse to proceed in distinct episodes.

[†]sean.p.long@wsu.edu

INTRODUCTION

The Basin and Range Province (Fig. 1A) is our finest modern example of large-scale continental extension. Decades of research have greatly expanded our knowledge of the structural mechanisms that accomplished Basin and Range extension (e.g., Anderson, 1971; Stewart, 1971; Armstrong, 1972; Wright and Troxel, 1973; Proffett, 1977; Wernicke, 1981; Zoback et al., 1981; Allmendinger et al., 1983; Gans and Miller, 1983; Miller et al., 1983; Coney and Harms, 1984; Gans, 1987; Faulds and Stewart, 1998; Dickinson, 2002; Colgan et al., 2006; Colgan and Henry, 2009; Long and Walker, 2015). Despite this progress, the structural complexity of the province has left several critical problems unresolved, including questions as fundamental as how much extensional strain has been accommodated in many areas of the province, and how strain has been distributed in space and time. The importance of this problem is augmented because Basin and Range extension is interpreted to have accommodated the collapse of an orogenic plateau constructed during Jurassic–Paleogene Cordilleran contractional deformation (e.g., Coney and Harms, 1984; Molnar and Lyon-Caen, 1988; Allmendinger, 1992; Dilek and Moores, 1999; DeCelles, 2004). Therefore, analysis of the magnitude and distribution of extension has the potential to inform us about the geodynamic mechanisms that contribute to the collapse of thickened crust. A detailed investigation of the geometric and kinematic framework of the Basin and Range Province is a critical prerequisite to begin addressing this problem.

Several researchers have estimated extensional strain using cross section reconstructions, most often from single ranges (e.g., Gans and Miller, 1983; Proffett and Dilles, 1984; Smith, 1992; Surpless et al., 2002; Colgan et al., 2008; Long et al., 2014a; Long and Walker, 2015), but sometimes spanning larger portions of the province (Bartley and Wernicke, 1984; Gans, 1987; Wernicke et al., 1988; Smith et al., 1991; Colgan et al., 2006; Colgan and Henry, 2009). Province-wide strain estimates have been obtained using map-view reconstructions that are supported by extension magnitudes compiled from individual ranges (Stewart, 1980; Coney and Harms, 1984; McQuarrie and Wernicke, 2005), and using paleomagnetic rotation magnitudes in the Sierra Nevada (Frei et al., 1984; Bogen and Schweickert, 1985). However, to date, a cross section that spans the full width of the province has not been presented.

The goal of this study is to illustrate the geometry and quantify the magnitude of extension across the Basin and Range by presenting a province-wide cross section centered at ~39°N. Retrodeformation of the cross section allows assessment of the spatial patterns of strain accumulation and provides a detailed view of the pre-extensional geometry. The reconstruction is integrated with newly published EarthScope crustal thickness data (Gilbert, 2012) in order to place constraints on pre-extensional crustal thickness, and how thicknesses may have varied from east to west. Implications for factors that may have controlled the distribution of extensional strain are then explored. Finally, a review of published extension timing constraints in proximity to the section line is presented, which allows placing extension in the temporal context of geodynamic driving mechanisms.

TECTONIC FRAMEWORK

From the Neoproterozoic to the Devonian, Nevada and western Utah were situated on the western Laurentian continental shelf, where a thick section of marine sedimentary rocks was deposited (e.g., Stewart and Poole, 1974; Poole et al., 1992). Following this, two obduction events, the Mississippian Antler orogeny and Permian–Triassic Sonoma orogeny, emplaced slope and basinal rocks eastward over the shelf edge in central and western Nevada (Fig. 1B; e.g., Speed and Sleep, 1982; Dickinson, 2000). In eastern Nevada and western Utah, shallow-marine deposition on the continental shelf continued until the Triassic (e.g., Stewart, 1980).

GSA Bulletin; January/February 2019; v. 131; no. 1/2; p. 99–119; https://doi.org/10.1130/B31974.1; 4 figures; 4 tables; Data Repository item 2018239; published online 15 August 2018.

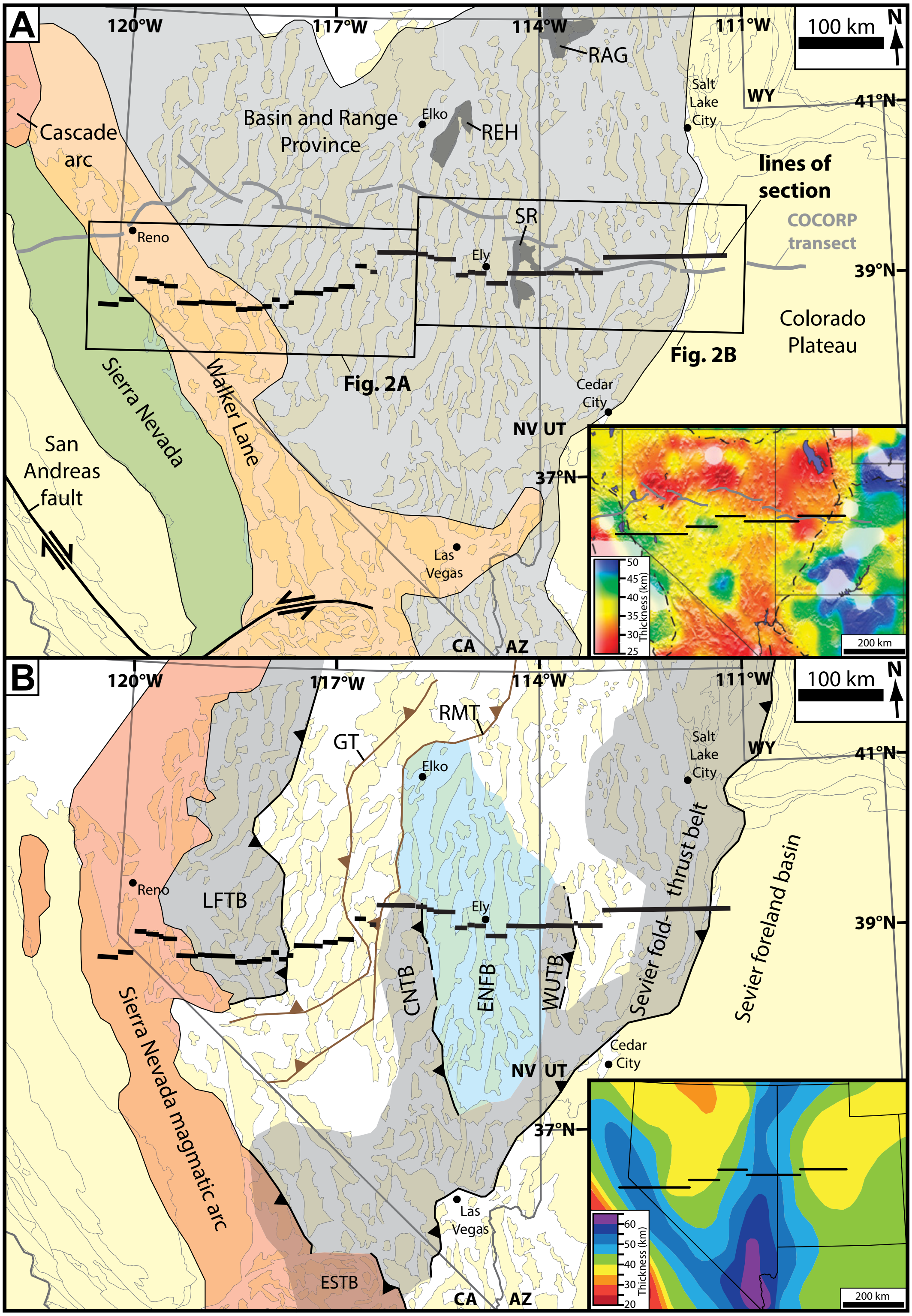

Figure 1. (A) Map of Utah, Nevada, and eastern California (base polygons from McQuarrie and Wernicke, 2005), showing Cenozoic tectonic provinces. Basin and Range boundaries are from Dickinson (2002) and Colgan et al. (2010). Walker Lane boundaries are from Faulds and Henry (2008). Location of Consortium for Continental Reflection Profiling (COCORP) transect is from Allmendinger et al. (1983). Inset shows EarthScope crustal thickness data (modified from Gilbert, 2012). Abbreviations: RAG—Raft River–Albion–Grouse Creek core complex; REH—Ruby–East Humboldt core complex; SR—Snake Range core complex. State abbreviations: WY—Wyoming, UT—Utah, NV—Nevada, AZ—Arizona, CA—California. (B) Map of same region as A, showing Mesozoic–Paleogene Cordilleran tectonic provinces (modified from Long, 2015). Inset shows approximate pre-extensional crustal thickness (modified from Coney and Harms, 1984; Best et al., 2009). Abbreviations: CNTB—Central Nevada thrust belt; ENFB—Eastern Nevada fold belt; ESTB—Eastern Sierra thrust belt; GT—Golconda thrust; LFTB—Luning-Fencemaker thrust belt; RMT—Roberts Mountains thrust; WUTB—Western Utah thrust belt.

During the Jurassic, closure of a back-arc basin in western Nevada constructed the E-vergent Luning-Fencemaker thrust belt (Fig. 1B; e.g., Oldow, 1984; Wyld, 2002). This established an Andean-style subduction system on the western North American margin, which initiated construction of the Cordilleran orogenic belt (e.g., DeCelles, 2004; Dickinson, 2004). Cordilleran provinces include the Jurassic–Cretaceous Sierra Nevada magmatic arc in California (e.g., Ducea, 2001), a broad hinterland region across Nevada, and the E-vergent Sevier thrust belt in western Utah (Fig. 1B), where a total of ~200 km of shortening was accommodated between the latest Jurassic and Paleogene (e.g., Burchfiel and Davis, 1975; DeCelles, 2004; Yonkee and Weil, 2015). In the hinterland, a few tens of kilometers of E-vergent shortening were accommodated within narrow thrust belts in central Nevada and western Utah and a broad region of folds in eastern Nevada (e.g., Gans and Miller, 1983; Taylor et al., 2000; Long, 2012, 2015; Greene, 2014).

Crustal shortening estimates, reconstructions of Cenozoic extension, and isotope paleoaltimetry suggest that 50–60-km-thick crust and 2.5–3.5 km elevations were attained in eastern Nevada during the Late Cretaceous and Paleogene (Coney and Harms, 1984; DeCelles and Coogan, 2006; Cassel et al., 2014; Snell et al., 2014), giving rise to the name "Nevadaplano," after comparison to the Andean Altiplano (e.g., Dilek and Moores, 1999; DeCelles, 2004). Evidence for localized, Late Cretaceous–Paleocene, synorogenic extension in the Nevadaplano has been documented, including normal faulting (Camilleri and Chamberlain, 1997; Druschke et al., 2009a; Long et al., 2015) and initial exhumation of midcrustal rocks now exposed in core complexes (Hodges and Walker, 1992; McGrew et al., 2000; Wells and Hoisch, 2008).

During the Paleocene and Eocene, eastward migration of shortening and magmatism into Utah and Colorado during the Laramide orogeny is interpreted to represent a shallowing of subduction angle (e.g., Dickinson and Snyder, 1978). This was followed by the Great Basin ignimbrite flare-up, a NE to SW magmatic sweep across Nevada and Utah between the late Eocene and early Miocene (e.g., Best et al., 2009; Henry and John, 2013), which is interpreted as a consequence of slab rollback (e.g., Humphreys, 1995). Volcanic rocks of the ignimbrite flare-up overlie Paleozoic–Mesozoic rocks across a regionally distributed Paleogene unconformity, which represents a postorogenic erosion surface that predates extension in most places (e.g., Armstrong, 1972; Gans and Miller, 1983; Long, 2012, 2015). In eastern Nevada and western Utah, some areas experienced Eocene–Oligocene extension (e.g., Gans et al., 1989, 2001; Potter et al., 1995; Constenius, 1996; Evans et al., 2015; Long and Walker, 2015; Lee et al., 2017). However, extension was localized, and paleoaltimetry data indicate that surface elevations were still high during this time (Wolfe et al., 1997; Horton et al., 2004; Cassel et al., 2014).

The inception of widespread extension that constructed the Basin and Range Province, and associated lowering of surface elevation (e.g., Colgan and Henry, 2009; Cassel et al., 2014), is attributed to reorganization of the Pacific–North American plate boundary in the middle Miocene, and more specifically to establishment of the San Andreas transform system (e.g., Atwater, 1970; Dickinson, 1997, 2002, 2006). The decrease in interplate coupling that accompanied the demise of Farallon plate subduction, and the corresponding increasing influence of dextral shear at the plate margin, remains the most widely accepted explanation for the primary driver of Basin and Range extension (e.g., Dickinson, 2002). Though the duration of extension spans from the Miocene to the present in most places, the timing, rates, and magnitudes of Basin and Range extension exhibit significant spatial variability (e.g., Gans and Miller, 1983; Dilles and Gans, 1995; Miller et al., 1999b; Colgan et al., 2006; Colgan and Henry, 2009).

METHODS

Individual cross sections of 18 ranges, spanning from the House Range in western Utah to the Carson Range in eastern California, were constructed using data from 36 published geologic maps, which were typically at scales between 1:24,000 and 1:62,500 (Table 1). These were integrated with a published cross section of the Sevier thrust belt in western Utah (DeCelles and Coogan, 2006), which extends from the House Range to the Wasatch Plateau. Deformed and restored versions of the province-wide cross section are presented on Plate DR1 at 1:200,000 scale.[1]

The lines of section through each range (Fig. 2) were selected to optimize the following criteria: (1) multiple across-strike exposures of the Paleogene subvolcanic unconformity, which is the datum used to restore extension; (2) extensive exposures of bedrock deformed by major normal fault systems, in order to yield the most information on extension; and (3) exposures of Paleozoic–Mesozoic thrust faults and fold axes, in order to constrain the pre-extensional deformation geometry. All three criteria were commonly met together only at one specific latitude in each range, which is the reason that the line of section is not a single continuous E-W trace.

Stratigraphic thicknesses were determined from geometric constraints along the line of section (i.e., dip angle and locations of contacts). When complete thicknesses could not be determined, thicknesses reported in source mapping or from the isopach maps of Stewart (1980) were utilized. Unit divisions were at the period level where possible, though grouping of units was necessary in some areas depending on the level of detail of source mapping. The sections were drafted down to the level of the lowest stratigraphic unit exposed in each range.

Apparent dips of attitude measurements from source maps (1412 measurements total; Table 1) were projected onto the cross section, and areas of similar apparent dip were divided into domains separated by kink surfaces (e.g., Suppe, 1983). Faults are shown as planar, and dip angles for some faults were calculated using three-point problems (Table DR1 [see footnote 1 for Table DR1 throughout]). In addition, many faults have published constraints on their geometries (e.g., Proffett and Dilles, 1984; Surpless et al., 2002; Long et al., 2014a), and many are constrained to a range of dip angles by their interactions with topography. However, the majority of faults on source maps either did not pass through sufficient topography, or their locations were not determined precisely enough to support three-point problems. Therefore, the majority of faults were assumed to have a 60° dip (e.g., Anderson, 1951), and their apparent dips were projected onto the cross section.

Geologic contacts offset across faults were drafted so that they were internally consistent and thus retrodeformable. Therefore, the cross sections represent viable (though nonunique) solutions (Elliott, 1983). For many normal faults, footwall cutoffs necessary for matching with subsurface hanging-wall cutoffs have been eroded. In these cases, geometries that minimized fault offset were used. Justifications for drafting decisions are annotated on Plate DR1 (see text footnote 1 for Plate DR1 throughout). The cross sections of individual ranges were retrodeformed by restoring offset on all normal faults and untilting the Paleogene unconformity to horizontal. The Paleogene unconformity was restored to an elevation of 3 km (e.g., DeCelles and Coogan, 2006; Cassel et al., 2014). Extension was estimated for each range by comparing present-day and pre-extensional lengths (Table 2). Assumption of 60° dip angles for many faults is likely the largest source of uncertainty in the restoration process. For example, for the idealized case of homogeneous, domino-style extension, using 50° and 70° fault dip angles would yield extension magnitudes that are ±4%, ±9%, and ±19% different than using 60° fault dip angles for 10°, 20°, and 30° of tilting, respectively (Wernicke and Burchfiel, 1982). However, because most of the examined ranges have experienced polyphase extension and exhibit differing fault dip directions, tilt directions, and tilt magnitudes, quantitative estimation of uncertainties for each range was not attempted.

In this study, no attempt was made to illustrate the deformation geometry of modern basins, because subsurface data that would allow quantification of extension magnitude are not available along the section line. Publicly available seismic reflection profiles of individual basins are limited in number, and they are mostly from northern Nevada (e.g., Anderson et al.,

[1]GSA Data Repository item 2018239, Plate DR1, Figure DR1, and Table DR1, is available at http://www.geosociety.org/datarepository/2018 or by request to editing@geosociety.org.

TABLE 1. GEOLOGIC MAP SOURCES USED TO SUPPORT SEGMENTS OF THE CROSS SECTION

Mountain range	Mapping source	Mapping scale	Latitude of section line (°N)	Longitude of western extent (°W)	Longitude of eastern extent (°W)	Number of measurements
Canyon Range to Wasatch Plateau	DeCelles and Coogan (2006)	1:860,000	39°21′25″	112°17′5″	111°23′5″	–
Sevier Desert Basin	DeCelles and Coogan (2006)	1:860,000	39°21′25″	113°31′15″	112°17′5″	–
House Range	Hintze (1974b)	1:48,000	39°12′35″	113°30′	113°15′	26
Confusion Range (E)	Hintze (1974a)	1:48,000	39°12′00″	113°45′	113°30′	30
Confusion Range (W)	Hose (1965)	1:24,000	39°12′00″	113°54′	113°45′	55
Northern Snake Range (E)	Miller and Gans (1999)	1:24,000	39°12′30″	114°07′30″	114°00′	47
Northern Snake Range (E-central)	Miller et al. (1999a)	1:24,000	39°12′30″	114°15′	114°07′30″	98
Northern Snake Range (W-central)	Johnston (2000)	1:24,000	39°12′30″	114°22′30″	114°15′	110
Northern Snake Range (W edge)	Hose and Blake (1976)	1:250,000	39°12′30″	114°24′45″	114°22′30″	0
Schell Creek Range	Drewes (1967)	1:48,000	39°05′30″	114°45′	114°30′	64
Egan Range (E)	Brokaw (1967)	1:24,000	39°12′45″, 39°12′15″	115°00′	114°52′30″	74
Egan Range (central)	Brokaw and Heidrick (1966)	1:24,000	39°10′50″, 39°12′45″	115°07′30″	115°00′	58
Egan Range (W)	Hose and Blake (1976)	1:250,000	39°10′50″	115°10′	115°07′30″	0
White Pine Range (E)	Hose and Blake (1976)	1:250,000	39°21′30″	115°22′30″	115°19′	0
White Pine Range (W and central)	Humphrey (1960)	1:48,000	39°21′30″	115°33′	115°22′30″	47
White Pine Range (W edge)	Tripp (1957)	1:40,000	39°22′45″	115°36′	115°33′	7
Pancake Range (E edge)	Tripp (1957)	1:40,000	39°24′35″	115°40′	115°39′	0
Pancake Range (W and central)	This study (Figure DR1)	1:12,000	39°24′35″	115°42′	115°40′	62
Diamond Mts./Fish Creek Range	Long et al. (2014a)	1:24,000	39°26′20″	116°6′	115°48′30″	192
Mahogany Hills	Schalla (1978)	1:24,000	39°26′15″	116°11′30″	116°6′	26
Monitor Range (E)	Bortz (1959)	1:24,000	39°13′10″, 39°14′30″	116°27′40″	116°22′	26
Monitor Range (central)	Roberts et al. (1967)	1:250,000	39°14′30″	116°29′10″	116°27′40″	0
Monitor Range (W)	Lohr (1965)	1:24,000	39°19′55″	116°35′15″	116°29′10″	18
Toquima Range	McKee (1976)	1:62,500	39°03′05″, 39°00′55″	117°00′	116°40′	47
Toiyabe Range	Cohen (1980)	1:20,000	38°58′15″	117°15′	117°12′	3
Toiyabe Range	Ferguson and Cathcart (1954)	1:125,000	38°58′15″	117°30′	117°07′30″	18
Shoshone Mountains	Whitebread et al. (1988)	1:62,500	38°51′30″, 38°48′55″	117°42′10″	117°30′	16
Paradise Range	John (1988)	1:24,000	38°53′10″, 38°48′30″, 38°46′45″	118°00′	117°42′10″	69
Paradise Range	Silberling and John (1989)	1:24,000	38°53′10″, 38°48′30″, 38°46′45″	118°00′	117°45′	37
Paradise Range (W)	Ekren and Byers (1986a)	1:48,000	38°46′45″	118°09′	118°00′	13
Gabbs Valley Range (E)	Ekren and Byers (1986a)	1:48,000	38°45′40″	118°15′	118°09′	6
Gabbs Valley Range (W)	Ekren and Byers (1986b)	1:48,000	38°45′40″, 38°49′25″	118°30′	118°15′	32
Gillis Range	Hardyman (1980)	1:48,000	38°49′25″	118°45′	118°30′	16
Wassuk Range/Gray Hills (E)	Bingler (1978)	1:48,000	38°49′45″, 38°48′35″	119°00′	118°45′	11
Wassuk Range/Gray Hills (E)	Stockli et al. (2002)	1:162,000	38°49′45″, 38°48′35″	119°02′25″	118°45′	17
Gray Hills (W)/Cambridge Hills	Stewart and Dohrenwend (1984)	1:62,500	38°48′35″	119°08′40″	119°00′	1
Singatse Range	Proffett and Dilles (1984)	1:24,000	38°59′20″	119°20′25″	119°08′40″	47
Buckskin Range	Stewart (1999)	1:100,000	39°00′35″	119°24′30″	119°20′25″	32
Pine Nut Mountains	Stewart (1999)	1:100,000	39°01′45″, 39°03′20″	119°45′	119°24′30″	43
Pine Nut Mountains	Cashman et al. (2009)	1:250,000	39°03′20″	119°41′30″	119°30′30″	7
Carson Range	Armin et al. (1983)	1:62,500	38°48′55″, 38°45′10″	120°00′	119°45′	35
Sierra Nevada	Loomis (1983)	1:62,500	38°45′10″	120°15′	120°00′	22
					Total measurements:	1412

Note: See text footnote 1 for Figure DR1.

1983). Gravity modeling has been used to estimate the depth to the base of valley fill and in some cases the offset magnitudes of intrabasinal faults (e.g., Cashman et al., 2009). However, gravity modeling does not constrain the deformation geometry of bedrock below the base of valley fill, or the offset magnitudes of normal faults that predate basin construction. Wells can constrain the depth of valley fill and bedrock contacts, but multiple across-strike wells in a single basin are required to constrain the geometry of subsurface normal faults. Publicly available well records from Nevada and Utah (Hess et al., 2004; Utah Department of Natural Resources, 2017) lack the spatial density to allow quantification of basin extension magnitude along the section line.

Here, I took a simple approach and assumed that the best available estimate of cumulative extension across a basin can be approximated by the extension magnitudes of the bounding ranges. For example, if one range records 50% extension, and the opposite range records 30%, then the intervening basin is interpreted to have accommodated 40% ± 10% extension. The basin was then retrodeformed accordingly, and an uncertainty magnitude was calculated (Table 2). This assumption is supported by evidence throughout much of the Great Basin showing that the modern system of basins and ranges formed during a relatively late phase of the protracted Cenozoic extension history (e.g., Zoback et al., 1981; Anderson et al., 1983; Gans et al., 2001; Colgan and Henry, 2009). I acknowledge that estimates obtained using this technique are approximate, and that the underlying assumption is more applicable to regions with higher extension magnitudes. This technique is likely to underestimate extension in basins that are situated between ranges that exhibit low extension magnitudes but that may be bound by relatively large-offset range-bounding faults. However, in the absence of the subsurface data necessary to provide more quantitative estimates, the technique implemented here is interpreted to provide a realistic first-order approximation.

Other assumptions and caveats include the following: (1) It is assumed that rock units are correctly identified, and that interpretations of stratigraphic versus structural contacts on all source maps are correct. (2) Though the extension direction was not oriented exactly E-W in many ranges (e.g., Lee et al., 1987; Faulds and Henry, 2008), and likely underwent temporal changes in several regions (e.g., Zoback et al., 1981, 1994; McQuarrie and Wernicke, 2005; Colgan, 2013), all section lines are oriented E-W, in order to estimate cumulative extension in a present-day longitudinal reference frame. (3) Drafting decisions were made to minimize extension, faults with offset magnitudes <100 m were typically not included, and extension estimates for basins that lie between low-extension (~10% or less) ranges are likely minima; therefore, the cumulative extension across the cross section should be regarded as a conservative estimate.

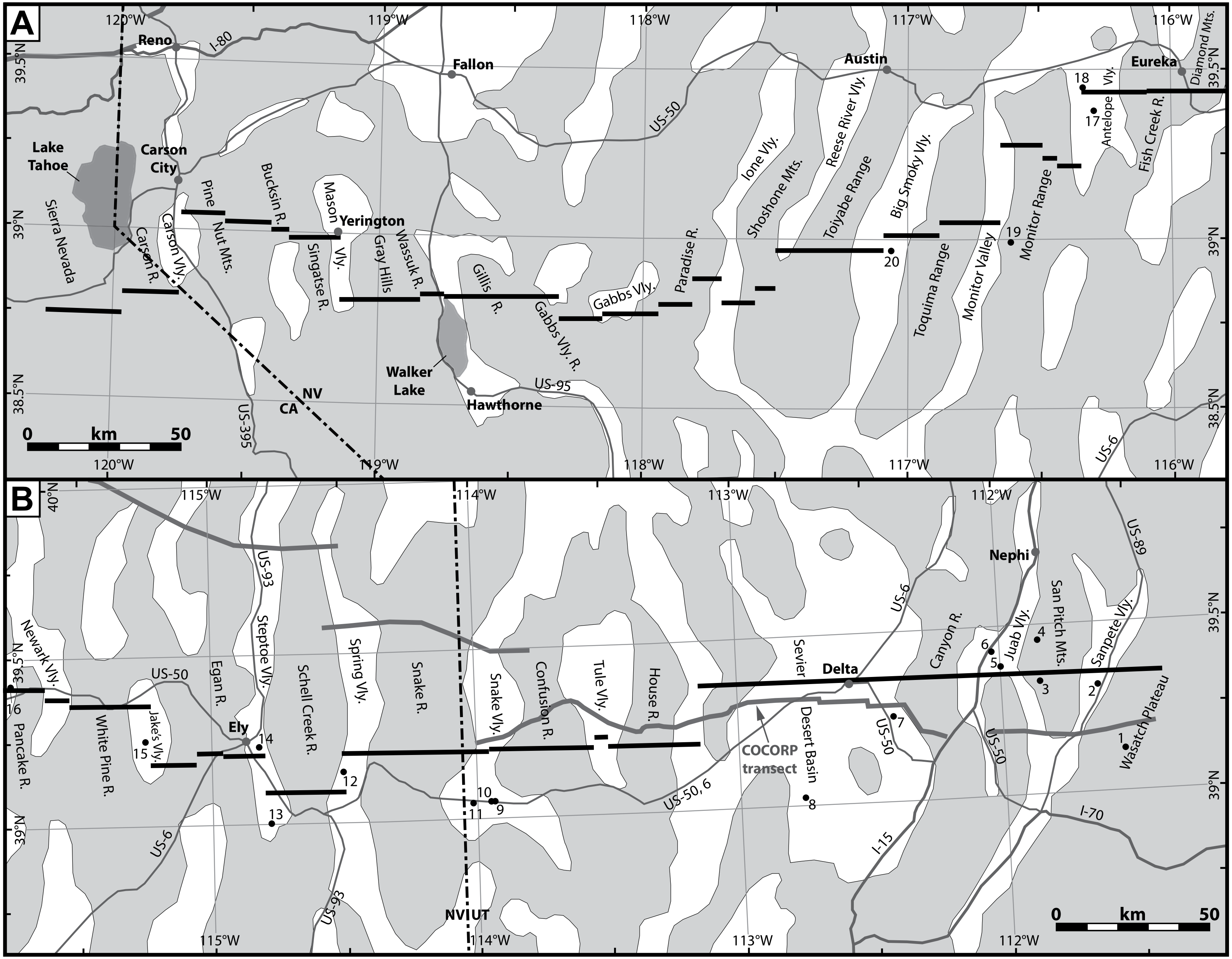

Figure 2. (A) Western and (B) eastern reference maps showing locations of lines of section (thick black lines) and guide to geographic names used in the text. Oil wells projected onto the cross section are shown with black dots (see guide to well numbering on Plate DR1). Location of Consortium for Continental Reflection Profiling (COCORP) transect (dark-gray lines) is from Allmendinger et al. (1983, 1987). Abbreviations: Mts—Mountains; R—Range; Vly—Valley. State abbreviations: UT—Utah, NV—Nevada, CA—California.

TABLE 2. SUPPORTING DATA FOR ESTIMATION OF EXTENSION

Mountain range or basin	Present-day length (km)	Pre-extensional length (km)	Extension (km)	Extension uncertainty (km)	Percent extension	Percent extension uncertainty
Wasatch Plateau to Canyon Range	71.2	64.3	6.9		11	
Sevier Desert Basin	84.5	50.6	33.9		67	
House Range	16.2	14.3	1.9		13	
Tule Valley	11.5	10.5	1.0	0.3	10	3
Confusion Range	26.2	24.4	1.8		7	
Snake Valley	14.6	8.9	5.7	4.7	129	122
Snake Range (strain estimate from footwall of NSRD)	30.6	8.7	21.9		250	
Spring Valley	7.1	3.0	4.1	1.0	164	86
Schell Creek Range	21.3	12.0	9.3		78	
Steptoe Valley	14.0	8.1	5.9	0.2	73	5
Egan Range	21.7	12.9	8.8		68	
Jake's Valley	14.0	10.4	3.6	2.1	41	28
White Pine Range	24.5	21.7	2.8		13	
Newark Valley (east)	4.4	4.0	0.4	0.1	10	3
Pancake Range	6.4	6.0	0.4		7	
Newark Valley (west)	7.1	5.7	1.4	1.0	29	22
Diamond Mts./Fish Creek R./Mahogany Hills	32.9	22.0	10.9		50	
Antelope Valley	15.6	12.3	3.3	1.9	30	20
Monitor Range	17.6	16.0	1.6		10	
Monitor Valley	10.4	9.6	0.8	0.2	8	2
Toquima Range	24.3	23.0	1.3		6	
Big Smoky Valley	22.5	20.7	1.8	0.6	9	3
Toiyabe Range	12.9	11.6	1.3		12	
Reese River Valley	9.9	9.1	0.8	0.3	9	3
Shoshone Mountains	9.5	9.0	0.5		6	
Ione Valley	10.2	6.8	3.4	2.8	80	74
Paradise Range	31.1	12.3	18.8		153	
Gabbs Valley	9.0	5.8	3.2	2.2	83	70
Gabbs Valley Range/Gillis Range	41.9	37.0	4.9		13	
Walker River Valley	7.5	4.7	2.8	2.0	98	85
Wassuk Range/Gray Hills/Cambridge Hills	27.9	9.9	18.0		182	
Mason Valley	7.3	2.6	4.7	0.1	181	2
Singatse Range/Buckskin Range	19.6	7.0	12.5		179	
Churchill Canyon	3.6	2.1	1.5	0.8	100	80
Pine Nut Mountains	24.9	20.8	4.1		20	
Carson Valley	3.0	2.6	0.4	0.1	16	5
Carson Range	17.0	15.3	1.7		11	
Total (no additional NSRD extension added)	**733.9**	**525.7**	**208.1**	**20.4**	**40**	**4**
Additional extension on NSRD (assuming 20°–40° dip range)			30	14		
Total (all additional 30 ± 14 km NSRD extension added)	**733.9**	**495.7**	**238.2**	**34.4**	**48**	**7**
Total (additional NSRD extension added as 22 ± 22 km range)	**733.9**	**503.8**	**230.1**	**42.4**	**46**	**8**

Note: NSRD—Northern Snake Range décollement.

In addition, because uncertainties were not estimated for restoration of ranges, all uncertainty estimates listed herein should also be interpreted as minima.

RANGE-BY-RANGE GEOMETRY AND EXTENSION MAGNITUDE (EAST TO WEST)

In this section, first-order normal faults are defined as having ≥1 km of offset, and second-order normal faults are defined as having <1 km of offset. Also, "steeply dipping" is defined as ≥50°, "moderately dipping" indicates dips between 20° and 50°, and "gently dipping" is defined as ≤20°. Extension magnitudes recorded in each range, as well as estimated extension magnitudes and uncertainties from basins, are listed in Table 2.

Wasatch Plateau to Sevier Desert Basin

The deformed and restored cross sections of DeCelles and Coogan (2006, their figs. 3 and 8F, respectively) were utilized for the 160-km-wide region from the Wasatch Plateau to the Sevier Desert Basin. Their study was focused on the kinematic development of the Sevier thrust belt; here, I focus primarily on implications for the geometry and magnitude of extension.

Between the latest Jurassic and Paleocene, the Sevier thrust belt accommodated ~220 km of shortening, which was distributed among four E-vergent thrust systems (Allmendinger et al., 1983; Villien and Kligfield, 1986; DeCelles et al., 1995; DeCelles and Coogan, 2006). The Canyon Range thrust, the structurally highest fault, carries an ~15-km-thick section of Neoproterozoic–Triassic rocks. To the east, the Pavant, Paxton, and Gunnison thrusts and associated duplex systems deform an ~3-km-thick section of Cambrian–Middle Jurassic sedimentary rocks, and a Late Jurassic–Cretaceous synorogenic section that is as thick as 6 km. At the deformation front, a W-vergent triangle zone deforms synorogenic rocks.

In the frontal portion of the thrust belt, between the Wasatch Plateau and Canyon Range, the cross section was restored so that the unconformity at the base of Paleogene sedimentary rocks is approximately horizontal. In the Wasatch Plateau, the unconformity dips 10°W, and three second-order normal faults sole into thrust faults of the frontal triangle zone. In Sanpete Valley, an ~20°W-dipping half graben formed from ~3 km of normal-sense motion on the Sanpete Valley back thrust. This basin contains tuffaceous rocks as old as ca. 39–27 Ma, and it represents one of a series of Eocene–Oligocene half grabens in this region that developed from extensional reactivation of thrust faults (Constenius, 1996). In the San Pitch Mountains, the Paleogene unconformity dips between 5°E and 5°W, and a second-order normal fault soles into the roof thrust of the Paxton duplex. In Juab Valley, a half graben containing 10°W- to 30°W-dipping Paleogene–Neogene rocks formed from 3 km of down-to-the-E offset on a normal fault that soles into the roof thrust of the Pavant duplex. Further west in Juab Valley, the Pavant thrust was reactivated with 1.5 km of normal offset. In the Canyon Range, the Paleogene unconformity is not exposed, and no normal faults intersect the section line. Comparison of final and initial widths from the Canyon Range to the Wasatch Plateau yielded 6.9 km (11%) of cumulative extension.

In the Sevier Desert Basin, the western portion of the thrust belt is buried under 1–5 km of Oligocene–Quaternary sediment. A 10°- to 20°W-dipping seismic reflector that can be traced under the basin for ~70 km has been interpreted as a low-angle extensional fault, the Sevier Desert detachment (e.g., Wernicke, 1981; Allmendinger et al., 1983, 1986, 1987; Allmendinger and Royse, 1995; Coogan and DeCelles, 1996; Stockli et al., 2001; DeCelles and Coogan, 2006). Alternatively, this reflector has been interpreted as an unconformity between Cenozoic and Paleozoic rocks (e.g., Anders and Christie-Blick, 1994; Anders et al., 1995, 2001). Here, I follow the detachment interpretation, after discussions in DeCelles and Coogan (2006) and Coogan and DeCelles (2007) that summarize structural, geophysical, well log, and sedimentologic data sets that require large-magnitude extension in this region of Utah. The Sevier Desert detachment is shown reactivating the Pavant and Paxton-Gunnison thrusts at depth, and a series of high-angle normal faults in the Sevier Desert Basin feed displacement into the detachment. Matching hanging-wall and footwall cutoffs indicate ~47 km of total displacement on the detachment. Comparison of the final and initial widths of the Sevier Desert Basin yielded 33.9 km (67%) of extension.

House Range

The House Range exposes subhorizontal Cambrian rocks and is deformed by a first-order, W-dipping normal fault system on its western flank and two second-order, E-dipping normal faults (Hintze, 1974b). Several across-strike exposures of the Paleogene unconformity, which underlies late Eocene tuff (ca. 35.4 Ma; Hintze and Davis, 2002), define minimal (≤3°) eastward tilting. Restoration of normal faults and tilting yielded 1.9 km of extension (13%).

The House Range occupies the crest of the Sevier culmination, a structural high defined by subvolcanic erosion levels (Harris, 1959; Hintze and Davis, 2003; Long, 2012) and arched reflectors on the Consortium for Continental Reflection Profiling (COCORP) profile (Allmendinger et al., 1983). The culmination is interpreted to have formed from duplexing of Precambrian crystalline basement, which folded the overlying Canyon Range thrust sheet (Allmendinger et al., 1987; DeCelles and Coogan, 2006).

Confusion Range

In the Confusion Range, Devonian–Permian rocks are deformed by the E-vergent Western Utah thrust belt, which accommodated ~10 km of shortening (Greene, 2014). In the western part of the range, several folds formed above the Brown's Wash thrust, including the Buckskin Hills detachment fold, which exhibits an overturned western limb (Greene, 2014). The eastern flank of the range is a gently W-dipping homocline in the hanging wall of the Payson Canyon thrust system, which ramps through Silurian–Devonian rocks (Hintze, 1974a; Greene, 2014). The ~8-km-wide region between the Knoll anticline and Conger Springs anticline is referred to as the Confusion synclinorium (Hose, 1977; Gans and Miller, 1983), a structural low that can be traced for a N-S distance of ~130 km (Long, 2012).

The Confusion Range is deformed by a series of second-order, E- and W-dipping, high-angle normal faults (Hose, 1965; Hintze, 1974a). Multiple across-strike exposures of the unconformity below late Eocene–Oligocene (ca. 35.4–30.5 Ma) volcanic and sedimentary rocks (Hintze and Davis, 2002) define ≤5° of eastward tilting. Restoration yielded 1.8 km of extension (7%).

Northern Snake Range

The Snake Range core complex has been extensively studied over the past 40 yr (e.g., Coney, 1974; Gans and Miller, 1983; Miller et al., 1983, 1999b; Bartley and Wernicke, 1984; Gans et al., 1985; Lee et al., 1987, 2017; Lee, 1995; Lewis et al., 1999; Cooper et al., 2010; Evans et al., 2015). However, many aspects of its development remain debated, in particular the tectonic significance of the E-vergent Northern Snake Range décollement, the primary extensional structure in the range. The principal disagreement is over the pre-extensional depth of Neoproterozoic–Cambrian metasedimentary rocks in the footwall of the décollement, and the corresponding implications for extension magnitude. Early, field-based studies proposed that the Northern Snake Range décollement originated as a subhorizontal zone of decoupling between brittlely deformed Cambrian–Permian sedimentary rocks in the hanging wall and ductilely attenuated Neoproterozoic–Cambrian metasedimentary rocks in the footwall that restore to pre-extensional stratigraphic depths of ~7–13 km (Gans and Miller, 1983; Miller et al., 1983; Gans et al., 1985; Lee et al., 1987). In contrast, other studies have made structural arguments (Bartley and Wernicke, 1984) and presented thermobarometry data (Lewis et al., 1999; Cooper et al., 2010) indicating that footwall rocks were buried as deep as ~23–30 km prior to extension and were exhumed by a much higher-offset (perhaps up to 60 km; Bartley and Wernicke, 1984) Northern Snake Range décollement.

Despite the results of the thermobarometry, this disagreement remains unresolved, as field relationships provide strong arguments that rocks above and below the Northern Snake Range décollement shared a common depositional, metamorphic, and intrusive history, and thus were stratigraphically contiguous prior to extension. These relationships (summarized in Miller et al., 1999b) include: (1) similar metamorphic grades observed above and below the Northern Snake Range décollement in several places; (2) correlation of distinct facies changes in Neoproterozoic–Cambrian rocks between the Northern Snake Range and surrounding ranges; (3) peak metamorphic conditions that increase gradually between the southern and northern Snake Range, with no sharp breaks observed; and (4) similarity in isotopic composition and age of Jurassic plutons between the Northern Snake Range and surrounding ranges. Resolution of this debate is beyond the scope of this paper. Instead, here I used geometric constraints from the cross section, published strain estimates, and published pressure-temperature (*P-T*) data to estimate a permissible offset magnitude range for the Northern Snake Range décollement, which is presented as an average and uncertainty that was factored into the cumulative extension estimate.

In the eastern two thirds of the range, two sets of normal faults are observed above the Northern Snake Range décollement (Miller and Gans, 1999; Miller et al., 1999a). The earlier set consists of gently W-dipping faults, which represent originally E-dipping normal faults that have been rotated to W dips (e.g., Miller et al., 1983). These faults are deformed by a younger set of steeply E-dipping faults that tilt Cambrian–Pennsylvanian rocks to typical dips of 25°–45°W. In the western third of the range, rocks above the Northern Snake Range décollement are deformed by one set of W-dipping normal faults that tilt Cambrian–Devonian rocks to typical dips of 20°E (Johnston, 2000). All normal faults in the range, with the exception of one second-order fault, terminate downward into the Northern Snake Range décollement.

The Paleogene subvolcanic unconformity is not exposed in this part of the Snake Range. However, Permian rocks are exposed in several localities within 5 km to the N and S of the section line (Miller et al., 1999a; Johnston, 2000), and they are the highest pre-extensional stratigraphic level preserved. Also, 35 km to the N, Oligocene volcanic rocks overlie Permian rocks, with a <5° difference in dip angle across the unconformity (Gans and Miller, 1983). Therefore, on the restored cross section, the unconformity is approximated as bedding parallel and lying within the Permian section (footnote 7 *in* Plate DR1).

On the cross section, the majority of fault-bounded blocks above the Northern Snake Range décollement contain Ordovician, Silurian, and Devonian rocks. The Ordovician–Devonian rocks preserved in all of these blocks were restored by placing them as close together as possible without overlapping. This yielded a 12.7 km minimum pre-extensional width for the Northern Snake Range décollement hanging wall, corresponding to 15.5 km of extension (122%). This estimate falls short of the 450%–500% extension estimated for the Northern Snake Range décollement hanging wall ~5 km to the north by Miller et al. (1983), though their extension magnitude (24.3 km) is of a similar order to my estimate. Much of this variation can be attributed to the difference in the relative ratios of preserved stratigraphic levels. My section line is dominated by Ordovician–Devonian rocks, whereas theirs contained an approximately even distribution of Cambrian to Pennsylvanian rocks. However, in light of these differing estimates, I chose to use published strain data from the footwall of the Northern Snake Range décollement (described below) as a more representative measure for estimation of extension.

In the footwall, Neoproterozoic–Cambrian metasedimentary rocks were deformed by coaxial stretching and thinning (e.g., Miller et al., 1983; Gans et al., 1985; Lee et al., 1987). All rocks exhibit a penetrative foliation that is subparallel to the Northern Snake Range décollement, and a WNW-trending stretching lineation, which decreases in intensity toward the west, eventually dying out at the western flank of the range (Gans et al., 1985). Rocks in the Northern Snake Range décollement footwall include the Cambrian Prospect Mountain Quartzite, which is attenuated to a thickness of <200 m in the eastern part of the range (Gans and Miller, 1983), and underlying metasedimentary rocks of the Neoproterozoic McCoy Creek Group (Miller and Gans, 1999). These units are intruded by Jurassic granite that is sheared concordant to foliation in the metasedimentary units (Miller et al., 1999a).

The magnitude of stretching in the footwall of the Northern Snake Range décollement was estimated by Lee et al. (1987), who integrated finite strain data with a comparison of the attenuated thickness of the Cambrian Prospect Mountain Quartzite to its undeformed regional thickness, which yielded an average extension estimate of 250%. On the restored cross section, widths were restored using this extension value, and unit thicknesses were restored to the average 1.2 km regional thickness of Cambrian quartzite (Miller et al., 1983; Lee et al., 1987) and the 5 km minimum thickness of Neoproterozoic rocks exposed in the Deep Creek Range 100 km to the N (Stewart, 1980). Using this strain magnitude, a total of 21.9 km of extension was accommodated by stretching and thinning.

Rocks in the footwall of the Northern Snake Range décollement are shown restored to a depth range of 7–13 km, after Miller et al. (1983). However, the ~23–30 km peak burial depth range obtained from thermobarometry (Lewis et al., 1999; Cooper et al., 2010) is also projected onto the cross section (footnote 4 *in* Plate DR1). Attainment of these depths has been interpreted as the result of Cretaceous structural thickening, with models ranging from burial by E-vergent thrust sheets in the western part of the Sevier thrust belt (Bartley and Wernicke, 1984) to W-vergent back thrusting (Lewis et al., 1999). Due to the large uncertainties in reconstructing the pre-extensional geometry at these depths, I took a simplified approach based on published constraints for the original dip angle of the Northern Snake Range décollement, including: (1) the 25°–30°E dip of the subsurface projection of the Northern Snake Range décollement on the COCORP profile (Allmendinger et al., 1983); (2) evidence for up to 40° of rotation of footwall rocks during exhumation, which implies that portions of the Northern Snake Range décollement dipped this steeply (Lee, 1995); and (3) the pre-extensional dip of 20°E shown on the structural models of Bartley and Wernicke (1984). Subsurface projections of the Northern Snake Range décollement are shown at 20°, 30°, and 40° dip angles, and their intersections with the peak burial range of footwall rocks yielded an offset range of 34 ± 13 km, which corresponds to an E-W extension magnitude of 30 ± 14 km.

Schell Creek Range

On the eastern flank of the Schell Creek range, ~20°W-dipping Cambrian–Ordovician rocks are deformed by several closely spaced, ~15°W-dipping (Table DR1), first-order faults that omit stratigraphy (Drewes, 1967), which are interpreted here as down-to-the-W normal faults. These faults are shown merging into one master fault (footnote 10 *in* Plate DR1). In the central and western parts of the range, E-dipping Devonian–Permian rocks above this master fault exhibit a hanging-wall cutoff angle of ~50°. To match this relationship in the footwall, the master fault was projected above the erosion surface to the east with an ~50° footwall cutoff angle (footnote 9 *in* Plate DR1). Therefore, the master fault is modeled as listric, with a high cutoff angle through Cambrian–Permian rocks and a flat near the base of the Cambrian section. In addition to the master fault, Devonian–Permian rocks in the western part of the range are also deformed by a series of dominantly W-dipping, first and second-order normal faults.

Eocene (ca. 36–35 Ma; Druschke et al., 2009b) sedimentary and volcanic rocks are exposed in the western and central parts of the range and dip 10°–25°E. The unconformity at their base cuts up section to the east, from Mississippian to Permian levels. Eocene rocks are cut by both low- and high-normal faults, and they do not overlap any normal faults (Drewes, 1967). Restoration of normal faults and tilting yielded 9.3 km of extension (78%). This is a minimum estimate, as matching cutoffs for the projected master normal fault were drafted to minimize extension. The pre-extensional geometry defines a 15°E-dipping homocline of Paleozoic rocks. Fifteen kilometers to the north, an ~4.5-km-thick section of Neoproterozoic–Lower Cambrian rocks is exposed on the eastern flank of the range (Young, 1960; Gans et al., 1985); these rocks were projected onto the cross section.

Egan Range

In the Egan Range, Pennsylvanian–Permian rocks are deformed by the Butte synclinorium, a NNW-trending structural low that can be traced along trend for 250 km (Hose, 1977; Gans and Miller, 1983; Long, 2012). The eastern part of the range is deformed by several W-dipping, second-order normal faults, and the E-dipping Eureka fault, which cuts Eocene rocks (Brokaw, 1967). In the central part of the range, the ~10°W-dipping (Table DR1) Kaibab fault has at least 4 km of offset, and field relations 5 km to the N of the section line show that motion on this fault predated late Eocene volcanism (Brokaw and Barosh, 1968; Gans et al., 2001). The W part of the range consists of gently dipping Pennsylvanian–Permian rocks that are deformed by an array of W- and E-dipping, second-order, high-angle normal faults (Brokaw and Heidrick, 1966). Eocene (Fouch et al., 1979; Gans et al., 2001) sedimentary and volcanic rocks dip 25°–45°E in the eastern part of the range (Brokaw, 1967) but change to a dip of 20°–25°W in the central part of the range (Brokaw and Heidrick, 1966). Retrodeformation yielded 8.8 km of extension (68%). The pre-extensional geometry defines the Butte synclinorium on this transect as a >12-km-wide, 5-km-tall, E-vergent syncline, with a western limb that dips as steeply as 75°E and an eastern limb that dips 30°–40°W.

White Pine Range

The White Pine Range exposes Mississippian–Permian rocks that are deformed by the N-trending Illipah anticline, Little Antelope syncline, and Emigrant anticline (Humphrey, 1960). The Illipah anticline, which can be correlated along trend for ~100 km (Long, 2015), is a tight fold with an eastern limb that dips as steep as ~50°–80°E and a western limb that dips as steep as ~50°W. In its western limb, an E-vergent thrust fault mapped by Humphrey (1960) places Mississippian rocks over Pennsylvanian rocks. To the west, the Little Antelope syncline and Emigrant anticline are open folds with limb dips of ~10°–30°.

The White Pine Range is deformed by steeply dipping, first- and second-order normal faults, which dip E on the western flank of the range and W in the central and eastern portions of the range (Tripp, 1957; Humphrey, 1960; Hose and Blake, 1976). Multiple across-strike exposures of Eocene–Oligocene volcanic and sedimentary rocks define minimal (≤3°) overall eastward tilting. Retrodeformation yielded 2.8 km of extension (13%).

Pancake Range

In the Pancake Range, Mississippian–Pennsylvanian rocks are deformed by an open syncline with ~20° limb dips (Fig. DR1). Paleogene volcanic rocks on the western side of the range dip 15°–20°W, but they are subhorizontal on the eastern side (Tripp, 1957; Fig. DR1). Two steeply dipping, second-order normal faults intersect the section line, and both offset Paleogene volcanic rocks. Retrodeformation yielded 0.4 km of extension (7%).

Diamond Mountains, Fish Creek Range, and Mahogany Hills

In the Diamond Mountains, Silurian–Mississippian rocks are deformed by the open Pinto Creek syncline and Sentinel Mountain syncline (Nolan et al., 1974; Long, 2015) and the E-vergent Moritz-Nager thrust (French, 1993). First-order normal faults include steeply dipping faults that bound a horst on the eastern side of the range, and the steeply W-dipping Pinto Summit fault, which all offset the basal unconformity of the Early Cretaceous Newark Canyon Formation, and which are all overlapped by late Eocene volcanic rocks (Long et al., 2014a).

In the Fish Creek Range, the steeply E-dipping Hoosac fault system and the steeply W-dipping Dugout Tunnel fault are overlapped by late Eocene volcanic rocks (Long et al., 2014a). In the western part of the range, Silurian–Devonian rocks are deformed by the Reese and Berry detachment system, consisting of two shallowly W-dipping faults that sole into a flat at the top of the Ordovician section, and that are cut by Eocene granite dikes (Cowell, 1986; Long et al., 2014a).

Retrodeformation of normal faults in the Fish Creek Range and Diamond Mountains reveals the Eureka culmination, a 20-km-wide, 5-km-tall open anticline. The culmination is interpreted as a fault-bend fold that formed from eastward displacement on the underlying Ratto Canyon thrust over a footwall ramp (Long et al., 2014a). The basal Newark Canyon Formation unconformity has been structurally elevated ~5 km across the E limb of the culmination, and the Newark Canyon Formation is folded in the hinge zone of the Pinto Creek syncline (Long, 2015). Long et al. (2014a) proposed that the Newark Canyon Formation was deposited in a piggyback basin that developed on the E limb of the culmination as it grew.

After its construction, the culmination was extended by two sets of first-order normal faults that predate ca. 37 Ma volcanism (Long et al., 2014a). The older set consists of oppositely dipping faults in each limb, including the Hoosac fault system and Reese and Berry detachment system. The younger set consists of steeply W-dipping normal faults, including the Pinto Summit and Dugout Tunnel faults, which accommodated 20°–30° of eastward tilting. Thermochronology data collected from Cambrian quartzite in the footwall of the Dugout Tunnel and Hoosac faults revealed rapid Late Cretaceous–Paleocene (ca. 75–60 Ma) cooling, which was interpreted to date the motion of both fault sets (Long et al., 2015). The Paleogene unconformity is presently subhorizontal, which indicates minimal extension since ca. 37 Ma (Long et al., 2014a).

In the Mahogany Hills, shallowly E-dipping Silurian–Devonian rocks are deformed by second-order, high-angle normal faults, and a shallowly W-dipping first-order normal fault that is overlapped by Paleogene volcanic rocks (Schalla, 1978). The Paleogene unconformity in the Mahogany Hills has undergone minimal (≤5°) westward tilting (Schalla, 1978).

Retrodeformation of all normal faults in the Mahogany Hills, Fish Creek Range, and Diamond Mountains yielded 10.9 km (50%) of extension. All first-order normal faults in these ranges are interpreted to be related to the Late Cretaceous–Paleocene extension event documented by Long et al. (2015). Therefore, because the Paleogene unconformity postdates extension, it was not restored to horizontal on Plate DR1. Rocks in these three ranges were retrodeformed to account for 20°–30° of eastward tilting of Late Cretaceous to late Eocene conglomerate in the Fish Creek Range that predated (or was contemporary with) extension (Long et al., 2014a). This restored the Paleogene unconformity to a westward dip (Plate DR1).

In the Mahogany Hills and Fish Creek Range, the E-vergent Roberts Mountains thrust, the basal structure of the Mississippian Antler orogeny (e.g., Speed and Sleep, 1982), was projected above the modern erosion surface (footnote 21 *in* Plate DR1). Fifteen kilometers north of the section line, the Roberts Mountains thrust places the Ordovician Vinini Formation over Mississippian rocks (Bentz, 1983). In the Fish Creek Range, Mississippian rocks are overlain by Permian rocks, and the Vinini Formation is not present (Nolan et al., 1974; Long et al., 2014a). Therefore, the Roberts Mountains thrust is shown tipping out at the contact between Mississippian and Permian rocks (footnote 20 *in* Plate DR1).

Monitor Range

Moderately W-dipping Ordovician–Devonian rocks are exposed on the east side of the Monitor Range (Bortz, 1959), and gently E-dipping Ordovician–Silurian rocks are exposed on the west (Lohr, 1965). In the E part of the range, the Roberts Mountains thrust is duplicated by a younger thrust fault that carries Ordovician rocks (Bortz, 1959). This fault is correlated with an E-vergent thrust mapped in the W part of the range (Lohr, 1965) that places Ordovician rocks over Silurian rocks.

The Paleogene subvolcanic unconformity dips 5°–10°E in the western part of the range, and it is subhorizontal in the eastern part (Bortz, 1959; Stewart and Carlson, 1978). The range is deformed by a series of E- and W-dipping, second-order normal faults, and restoration yielded 1.6 km of extension (10%). Volcanic rocks are cut by normal faults and do not overlap them.

Toquima Range

In the eastern Toquima Range, gently W-dipping Ordovician–Devonian rocks underlie the Roberts Mountains thrust, which carries the Ordovician Vinini Formation. In the footwall of the Roberts Mountains thrust, an E-vergent thrust fault was mapped that places Ordovician rocks over Devonian rocks (McKee, 1976). This thrust fault is shown cutting the Roberts Mountains thrust above the erosion surface.

The unconformity at the base of early Oligocene (ca. 32.3–30.1 Ma) volcanic rocks dips

2°–10°W in the western half of the range and 10°E in the eastern half (McKee, 1976). The range is deformed by E- and W-dipping, second-order normal faults, and retrodeformation yielded 1.3 km of extension (6%). Oligocene volcanic rocks are cut by normal faults and do not overlap them.

Toiyabe Range

The Toiyabe Range exposes steeply W-dipping Cambrian, Ordovician, and Permian rocks in the footwall of the E-vergent Golconda thrust, the basal structure of the Permian–Triassic Sonoma orogeny (Ferguson and Cathcart, 1954; Stewart and Carlson, 1978). The Golconda thrust carries the Mississippian–Permian Havallah Formation, which consists of volcanic rocks interlayered with pelagic sedimentary rocks (Ferguson and Cathcart, 1954; Babaie, 1987).

Oligocene volcanic rocks dip 15°W in the western part of the range (Table DR1). At this latitude, the Toiyabe Range is deformed by a single first-order, steeply W-dipping normal fault (Ferguson and Cathcart, 1954). Restoration yielded 1.3 km of extension (12%).

Shoshone Mountains

In the Shoshone Mountains, Triassic–Jurassic sedimentary and volcanic rocks dip gently W in the eastern part of the range, but they are steeply dipping and deformed by E-dipping thrust faults in the western part of the range (Stewart and Carlson, 1978; Kleinhampl and Ziony, 1985; Whitebread et al., 1988). This transition demarcates the eastern limit of the Luning-Fencemaker thrust belt (Oldow, 1984). Here, the leading portion of the thrust belt is modeled as a triangle zone, with steeply E-dipping Triassic–Jurassic rocks being carried by W-vergent thrust faults, and a frontal, W-vergent, overturned fold interpreted to have formed above a blind thrust fault.

The Oligocene subvolcanic unconformity dips 2°–3°W. Three second-order normal faults intersect the section line, and retrodeformation yielded 0.5 km of extension (6%). Oligocene volcanic rocks as young as ca. 24.4 Ma are cut by normal faults (Whitebread et al., 1988).

Paradise Range

In the Paradise Range, Triassic–Jurassic sedimentary and volcanic rocks are overlain by Oligocene–early Miocene tuffs and lavas (Ekren and Byers, 1986a; John, 1988; Silberling and John, 1989). The range records evidence for high-magnitude, domino-style extension accommodated by two first-order, down-to-the-W normal faults that presently dip 0–15°W. In the E part of the range, volcanic rocks dip ~25°E (John et al., 1989) and are cut by a gently W-dipping normal fault that is here correlated with the Paradise fault mapped in the central part of the range by Silberling and John (1989). In the W part of the range, volcanic rocks dip ~30°–45°E (Ekren and Byers, 1986a; Silberling and John, 1989) and are cut by the gently W-dipping Sheep Canyon fault. The Sheep Canyon and Paradise faults have offset magnitudes of 12 and 8 km, respectively. In addition, a series of younger, E- and W-dipping, high-angle, first- and second-order normal faults also deform the range. Restoration yielded 18.8 km of extension (153%). Retrodeformation of the Paradise and Sheep Canyon faults restores their original dips to 40°–50°W.

Triassic and Jurassic rocks in the Paradise Range occupy the central portion of the Luning-Fencemaker thrust belt and exhibit complex deformation geometries. Many Triassic–Jurassic stratigraphic units are grouped together on source maps, and their dips commonly change over short distances from upright to overturned, implying common mesoscale folding. In addition, large areas of Triassic–Jurassic exposures contain no measurements on source maps. Therefore, all Triassic–Jurassic units in the Paradise Range are shown as undifferentiated, and no attempt was made to illustrate their structural geometry. However, the E-vergent Gabbs and Holly Wells thrusts mapped by Silberling and John (1989) are shown, which dip 20°–45°W after restoration of extension.

Gabbs Valley Range and Gillis Range

The Gabbs Valley and Gillis Ranges occupy the central portion of the Walker Lane province and contain four fault systems (Petrified Spring, Benton Springs, Gumdrop Hills, and Agai Pah Hills faults) that have accommodated ~40 km of cumulative dextral offset (Ekren and Byers, 1984; Hardyman, 1984; Faulds and Henry, 2008). No attempt was made to retrodeform dextral offset. Instead, the cumulative restored length of packages of rock between these strike-slip faults was used to estimate extension, similar to the technique used in all other ranges.

In the Gabbs Valley Range, ~30°E-dipping Oligocene–early Miocene volcanic rocks overlie Triassic sedimentary and volcanic rocks (Ekren and Byers, 1986a). In the Gillis Range, Oligocene–Miocene volcanic rocks dip ~20°E, and on the W flank of the range, they dip ~20°W (Hardyman, 1980; Ekren and Byers, 1986b). Both ranges are deformed by steeply W-dipping, first- and second-order normal faults, and retrodeformation yielded 4.9 km of extension (13%).

In the Gillis Range, Hardyman (1980) mapped all contacts between pre-Cenozoic rock units and Oligocene–Miocene volcanic rocks as low-angle normal faults and interpreted them to be related to dextral faulting. However, as no information is available on their motion sense, and their existence has been disputed by Eckberg et al. (2005), who mapped them as unconformities, offset on these faults was not incorporated into the estimation of extension (footnote 34 *in* Plate DR1).

Wassuk Range, Gray Hills, and Cambridge Hills

The Wassuk Range, Gray Hills, and Cambridge Hills record evidence for high-magnitude domino-style extension (discussed in detail in Surpless et al., 2002; Stockli et al., 2002; Surpless, 2012). Oligocene–middle Miocene volcanic rocks, which were deposited atop Jurassic–Cretaceous granitic plutons and Triassic metavolcanic rocks, have been tilted to dips of 45°–60°W, with rotation accommodated by motion on closely spaced, first-order, down-to-the-E faults that presently dip 10°–15°E (Bingler, 1978; Stewart and Dohrenwend, 1984). A younger set of second-order, steeply E-dipping normal faults cuts the older normal faults. Retrodeformation yielded 18.0 km of extension (182%), which is similar to the ~200% estimate of Surpless (2012).

Singatse Range and Buckskin Range

The Singatse and Buckskin Ranges represent a classic example of high-magnitude, domino-style extension (Proffett, 1977; Proffett and Dilles, 1984). Here, Oligocene–middle Miocene volcanic rocks, which were deposited atop Jurassic granitic plutons containing roof pendants of Jurassic metavolcanic rocks, have been tilted to dips of ~60°W. Tilting was accommodated by first-order normal faults that started out at 60°–70°E dip angles but were rotated to dips of 5°–15°E (Proffett and Dilles, 1984; Stewart, 1999). A younger generation of steeply E-dipping, first- and second-order normal faults cuts the older fault set. Restoration yielded 12.5 km of extension (179%), which is in agreement with the >150% estimate of Proffett (1977).

Pine Nut Mountains

In the eastern part of the Pine Nut Mountains, ~35°W-dipping Oligocene tuffs overlie Jurassic granite plutons that contain roof pendants of Jurassic metavolcanic rocks (Stewart, 1999). In the western part of the range, 15°–30°W-dipping late Miocene (ca. 7–2 Ma) sedimentary rocks of the Gardnerville Basin (Cashman et al.,

2009) overlie Jurassic–Cretaceous granite plutons and Jurassic roof pendants (Stewart, 1999). The range is deformed by steeply E-dipping, first- and second-order normal faults, and retrodeformation yielded 4.1 km of extension (20%).

Carson Range

In the Carson Range, ~5°W-dipping Oligocene–Miocene volcanic rocks overlie Cretaceous granite plutons and Triassic–Jurassic metavolcanic rocks (Armin et al., 1983). The range is deformed by four steeply E-dipping, first- and second-order normal faults, and a steeply W-dipping second-order normal fault demarcates the western limit of extension. Retrodeformation yielded 1.7 km of extension (11%). To the west, the Sierra Nevada range is dominated by Cretaceous granitic rocks (Loomis, 1983), and multiple across-strike exposures of Oligocene–Miocene volcanic rocks define a 2°W average dip for their basal unconformity (Loomis, 1983).

DISCUSSION

Implications of Extension Magnitude for Pre-Extensional Crustal Thickness

The present-day length of the cross section between the E and W limits of extension is 733.9 km (Table 2). Assuming that rocks in the footwall of the Northern Snake Range décollement restore to stratigraphic depths of 7–13 km (Miller et al., 1983), which is the geometry shown on Plate DR1, 208.1 ± 20.4 km of cumulative extension (40% ± 4%) can be measured on the cross section. However, an additional 30 ± 14 km of extension (see discussion above) would be required when taking into account thermobarometry data from rocks in the footwall of the Northern Snake Range décollement (Cooper et al., 2010). Since data and field relations have been presented that support both end-member scenarios for the Northern Snake Range décollement, here I add in this additional extension as an average and uncertainty (22 ± 22 km; Table 2). This yields 230.1 ± 42.4 km of cumulative extension (46% ± 8%), which is interpreted to be a more representative estimate, as it is compatible with these differing structural models. This estimate is in agreement with estimates from map-view reconstructions, which range between ~42% (Coney and Harms, 1984) and ~50% (McQuarrie and Wernicke, 2005) along the latitude of the cross section, and an ~52% estimate at 39°N from paleomagnetic data from the Sierra Nevada (Bogen and Schweickert, 1984). This estimate is also similar to cumulative extension estimates further to the south in the Basin and Range, between ~36°N and 37°N, which range from 215 to 300 km (Snow and Wernicke, 2000; McQuarrie and Wernicke, 2005). However, the percent extension at these latitudes is much larger, at ~200% (McQuarrie and Wernicke, 2005).

Crustal thickness data from the EarthScope USArray (Gilbert, 2012), which are constrained by 17 proximal seismic stations across the width of the cross section (Fig. 3B), define an average modern thickness of 37 ± 1 km. Assuming that the lower crust was homogeneously extended and thinned by the same magnitude as the upper crust (e.g., Gans, 1987; Colgan et al., 2006), restoration of cumulative extension across the province yields an average pre-extensional thickness of 54 ± 6 km (Table 3). This is interpreted as a maximum thickness, as it does not account for any rock that was potentially added to the base of the crustal column during Cenozoic magmatism. Studies in other areas of the Great Basin have estimated as much as ~5 km of crustal addition from magmatic underplating (Gans, 1987; Catchings, 1992). However, since the amount that was added along the section line (if any) is not known, it was not factored into the estimate. This estimate is similar to the 55–65 km crustal thickness proposed to have been attained across the Cordilleran retroarc based on isotopic ratios from granitic plutons (Chapman et al., 2015), but it is greater than the ~45 km average thickness estimated at ~40°N using mass balance considerations (Colgan and Henry, 2009). However, most of this difference can be attributed to N-S variations in present-day crustal thickness (Gilbert, 2012). At 39°N, the crust is in most places ~5 km thicker, and in some places up to ~10 km thicker, than at 40°N–41°N (Fig. 1A). This is also illustrated on Plate DR1, which allows direct comparison of Moho depth from the COCORP seismic profile at ~40°N and the EarthScope thickness data along the section line.

Additional details on potential E-W variations in pre-extensional crustal thickness can be gained by analyzing spatial patterns of high- and low-magnitude average extension. The cross section can be divided into four distinct domains (Fig. 3C; Table 3): (1) the Wasatch Plateau to the Canyon Range (11% extension); (2) the Sevier Desert Basin to Antelope Valley (66% ± 16%); (3) Antelope Valley to Ione Valley (11% ± 3%); and (4) Ione Valley to the Carson Range (60% ± 5%). Assuming that lower-crustal extension and thinning were equal in magnitude to upper-crustal extension (e.g., Colgan et al., 2006), significant thickness differences are implied; domains 1 and 3 restore to 39 ± 1 km and 41 ± 3 km, respectively, and domains 2 and 4 restore to 60 ± 11 and 66 ± 5 km, respectively (Fig. 3D). Interpreting these differences as geologically meaningful requires an additional assumption that E-W and N-S thickness differences were not significantly evened out by lower-crustal flow. In any case, the differences implied by this simple reconstruction should be considered maxima. However, the two high-extension domains can be related spatially to portions of the Cordilleran orogenic belt that are predicted to have the thickest crust.

Domain 1 (Wasatch Plateau to Canyon Range) lies within the frontal portion of the Sevier thrust belt, where relatively minimal thickening (between 5 and 8 km; measured by summing the vertical thickness above the top of the undeformed, pre-orogenic sedimentary section) was accomplished by synorogenic deposition and structural duplication of an ~3-km-thick section of pre-orogenic rocks (DeCelles and Coogan, 2006). The 39 ± 1 km restored thickness of domain 1 is compatible with minimal thickening and is similar to the present-day 42 ± 1 km crustal thickness of the Colorado Plateau to the east (Gilbert, 2012).

Domain 2 (Sevier Desert Basin to Antelope Valley) includes the western portion of the Sevier thrust belt and a wide region of its hinterland. Its eastern boundary lies near the trace of the Canyon Range thrust, which delineates the eastern limit of significant crustal thickening, accommodated by two main processes: (1) translation of the thick passive-margin basin section eastward over the Wasatch hinge line, a narrowly defined zone in western Utah across which the Neoproterozoic–Triassic section increases in thickness from ~3 to >15 km, and which is interpreted to mark the eastern limit of Neoproterozoic rifting of North American continental crust (e.g., Poole et al., 1992); and (2) westward underthrusting of an ~220 km length of unrifted North American continental crust, which is a kinematic requirement of the shortening recorded in the Sevier thrust belt (Fig. 3E; e.g., DeCelles and Coogan, 2006; DeCelles et al., 2009).

Across westernmost Utah and eastern Nevada, evidence for significant upper-crustal thickening is lacking, and the cumulative magnitude of shortening accommodated by folding and thrust faults is estimated at only a few tens of kilometers (Taylor et al., 2000; Greene, 2014; Long, 2012, 2015). However, the underthrusting of unrifted continental crust can account for significant crustal thickening of this region. Underthrusting can account for at least ~12 km of addition to the crustal column under eastern Nevada and westernmost Utah (estimated from the difference in basin thickness across the Wasatch hinge line). This estimate is likely a minimum, as it does not account for any potential synorogenic lower-crustal thickening.

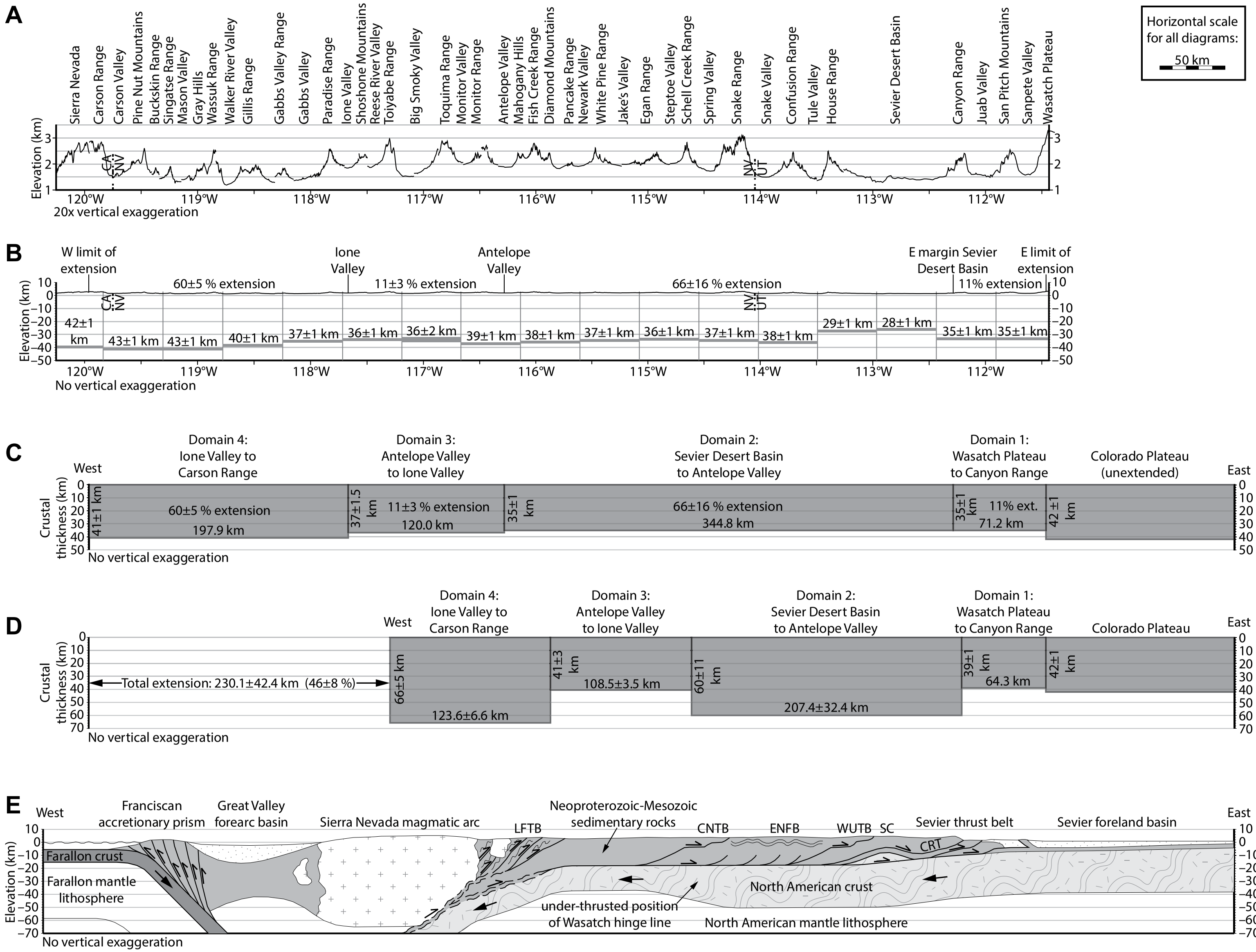

Figure 3. (A) Topography of the cross section line, shown with 20× vertical exaggeration. (B) Present-day crustal thicknesses along the cross section, as constrained by EarthScope USArray seismic stations (Gilbert, 2012). (C) Present-day widths and average crustal thicknesses of the four extension domains, and the western portion of the Colorado Plateau. (D) Restored, pre-extensional widths and average crustal thicknesses of the four extensional domains. (E) Schematic cross section of the Cordilleran orogenic belt at the latitude of the section line, showing predicted east-west variations in crustal thickness. The portion west of the Sierra Nevada magmatic arc is modified from DeCelles and Coogan (2006). The approximate underthrusted position of the Wasatch hinge line is shown (see text for details). Abbreviations: CNTB—Central Nevada thrust belt; CRT—Canyon Range thrust; ENFB—Eastern Nevada fold belt; LFTB—Luning-Fencemaker thrust belt; SC—Sevier culmination; WUTB—Western Utah thrust belt. State abbreviations: UT—Utah, NV—Nevada, CA—California.

TABLE 3. DATA SUPPORTING ESTIMATION OF PRE-EXTENSIONAL CRUSTAL THICKNESS

Extension domain	Present-day length (km)	Average present-day thickness (km)	Cross-sectional area (km^2)	Extension (km)	Percent extension	Pre-extensional length (km)	Pre-extensional thickness (km)
Domain 1: Wasatch Plateau to Canyon Range	71.2	35.00 ± 1.00	2490 ± 70	6.9	11	64.3	39 ± 1
Domain 2: Sevier Desert Basin to Antelope Valley	344.8	35.00 ± 1.00	12070 ± 345	137.5 ± 32.4	66 ± 16	207.4 ± 32.4	60 ± 11
Domain 3: Antelope Valley to Ione Valley	120.0	36.75 ± 1.50	4410 ± 180	11.5 ± 3.5	11 ± 3	108.5 ± 3.5	41 ± 3
Domain 4: Ione Valley to Carson Range	197.9	40.75 ± 1.00	8065 ± 200	74.3 ± 6.6	60 ± 5	123.6 ± 6.6	66 ± 5
Full width of Basin and Range Province	733.9	36.75 ± 1.00	26970 ± 735	230.1 ± 42.4	46 ± 8	503.8 ± 42.4	54 ± 6

Notes: Average present-day thickness and associated uncertainty were calculated from data presented in Gilbert (2012); values were rounded to nearest 0.25 km. Cross-sectional area and associated error were rounded to nearest 5 km^2. Pre-extensional thickness was calculated by assuming lower crust was homogeneously extended and thinned by same magnitude as upper crust. Pre-extensional thickness and associated uncertainty were rounded to nearest 1 km.

Based on the shortening accommodated in the Sevier thrust belt, the matching hanging-wall (i.e., within the Sevier thrust belt) and footwall (i.e., beneath the basal Sevier décollement) positions of the hinge line should be separated by ~220 km. In the Sevier thrust belt, the eastern part of the hinge line has been eroded in the leading edge of the Canyon Range thrust sheet, but the westernmost portion lies above the Canyon Range culmination (DeCelles and Coogan, 2006). The corresponding underthrusted position restores approximately below the Fish Creek Range, which is the near the western boundary of domain 2 (Fig. 3E). Therefore, the difference in pre-extensional thickness between domains 2 and 3 can likely be attributed to the western limit of unrifted North American continental crust. Significant E-W differences in the thickness of underthrusted crust have also been invoked to explain similar changes in orogenic architecture in the hinterland of the Cordilleran thrust belt in Canada (e.g., Price, 1981; Evenchick et al., 2007).

The 66% ± 16% average extension across domain 2 is comparable to published estimates from map-view reconstructions (~70% through easternmost Nevada; Coney and Harms, 1984) and from regional cross sections at 40°N (55%–77%; Gans, 1987; Smith et al., 1991). The 60 ± 11 km pre-extensional thickness obtained for domain 2 is within error of most published estimates for eastern Nevada, which range from 45 to 60 km (Coney and Harms, 1984; Gans, 1987; Smith et al., 1991; DeCelles and Coogan, 2006; Colgan and Henry, 2009).

Domain 3 (Antelope Valley to Ione Valley) lies within a region affected by late Paleozoic contractional deformation (the Antler and Sonoma orogenies). Along the cross section, E-vergent thrust faults with kilometer-scale offset that cut the Roberts Mountains thrust have been mapped in the Monitor and Toquima Ranges (Bortz, 1959; Lohr, 1965; McKee, 1976) and could be of Cordilleran age. However, the lack of regionally traceable thrust faults, significant erosion, or development of significant structural relief that postdates the Antler and Sonoma events indicates that this was a region of limited upper-crustal shortening during Cordilleran orogenesis (e.g., Speed, 1983; Speed et al., 1988; Smith, 1992). The 41 ± 3 km restored thickness for domain 3 is similar to the ~45 km estimate of Colgan and Henry (2009) ~100 km along strike to the north.

Domain 4 (Ione Valley to Carson Range) includes the Luning-Fencemaker thrust belt and the eastern portion of the Sierra Nevada magmatic arc. The Luning-Fencemaker thrust belt accommodated significant shortening (55%–75%; estimated in NW Nevada) through thrusting, folding, and fabric development in Triassic and Jurassic basinal rocks (Wyld, 2002; Wyld et al., 2003). Integrating this estimate over the ~40 km restored width of the Luning-Fencemaker thrust belt on the cross section indicates the potential for ~50–120 km of shortening. Therefore, the boundary between the Luning-Fencemaker thrust belt and the little-deformed region to the east, which corresponds approximately with the boundary between domains 3 and 4, is the site of another predicted E-W difference in crustal thickness during Cordilleran orogenesis.

West of the Luning-Fencemaker thrust belt, from the Gillis Range to the Sierra Nevada, exposures are dominated by Jurassic–Cretaceous granite of the Sierran magmatic arc. The primary mechanism for crustal thickening here was growth of the Cordilleran arc system, which was fueled by underthrusting of continental crust from the east (e.g., Saleeby et al., 2003; DeCelles et al., 2009). The 66 ± 5 km restored thickness of domain 4 is comparable to ~70 km crustal thickness estimates obtained from barometric analyses of xenoliths from the southern Sierran arc, which consisted of an ~30–35-km-thick granitic batholith complex underlain by a ~35–40-km-thick root of eclogitic residues (Ducea and Saleeby, 1998; Ducea, 2001; Saleeby et al., 2003). Present-day crustal thicknesses in the Sierra Nevada to the west of the cross section are thinner (42 ± 1 km; Gilbert, 2012), which has been attributed to late Miocene–Pliocene delamination of the eclogitic root (Ducea and Saleeby, 1998; Saleeby et al., 2003). The ~66 km restored thickness of domain 4 suggests that the eastern portion of the arc at this latitude thinned largely as a result of high-magnitude extension, with delamination perhaps playing a more limited role.

Space-Time Patterns of Extension, and Implications for Driving Mechanisms

The geodynamic influences that led to extension of thickened Cordilleran crust have been the subject of long-standing debate (e.g., Coney and Harms, 1984; Sonder and Jones, 1999; Colgan and Henry, 2009; Cassel et al., 2014). Many have argued that most of the widening of the Basin and Range Province was accomplished from the middle Miocene to the present (e.g., Zoback et al., 1994; Miller et al., 1999b; Stockli et al., 2001; Dickinson, 2002, 2006; Surpless et al., 2002; Colgan et al., 2006, 2010; Faulds and Henry, 2008; Colgan and Henry, 2009; Henry et al., 2011), which has been attributed to organization of the San Andreas transform into a through-going strike-slip system on the southern California coast by ca. 17 Ma (e.g., Atwater, 1970; Dickinson, 2002; Faulds and Henry, 2008). Therefore, the decreasing influence of interplate coupling that accompanied the transition from Andean-type subduction to a transform boundary is interpreted as the principal geodynamic trigger that facilitated widespread collapse of thick Cordilleran crust (e.g., Dickinson, 2002). However, several studies have also presented evidence for earlier, spatially isolated extension, including during the Late Cretaceous–Paleocene terminal stages of Cordilleran shortening (e.g., Hodges and Walker, 1992; Camilleri and Chamberlain, 1997; McGrew et al., 2000; Wells and Hoisch, 2008; Druschke et al., 2009a; Wells et al., 2012; Long et al., 2015), and during the Eocene–early Miocene ignimbrite flare-up (e.g., Gans and Miller, 1983; Gans, 1987, 2001; John et al., 1989; Dilles and Gans, 1995; Druschke et al., 2009b; Long and Walker, 2015). In order to explore potential geodynamic influences on the space-time patterns of extension, published timing constraints within ~100 km N or S of the cross section line were graphed versus longitude on Figure 4.

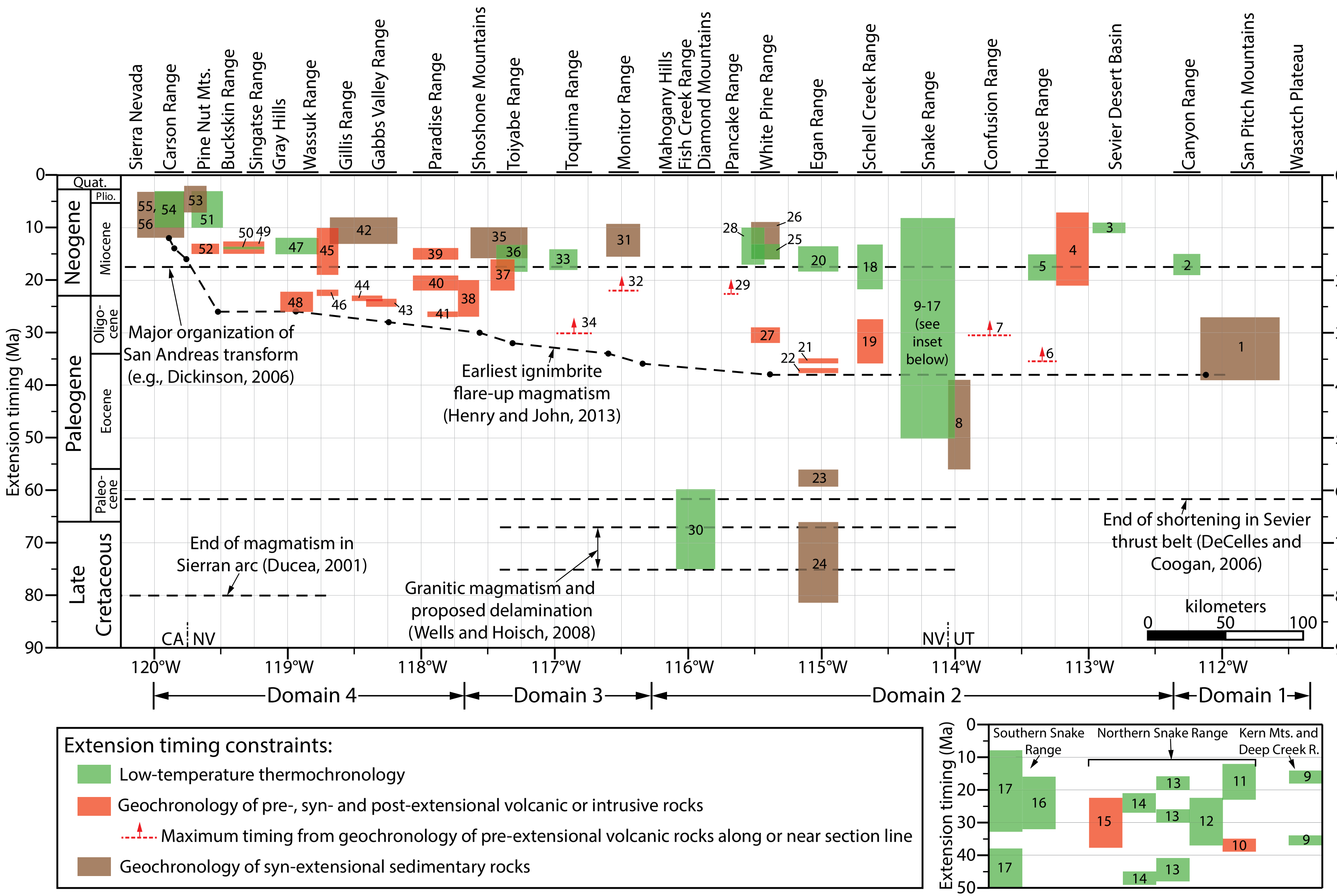

Figure 4. Compilation of published extension timing constraints within ~100 km north or south of the section line, plotted versus longitude (numbers correspond to studies in Table 4). Geochronology of volcanic rocks (red boxes) in many places only brackets the timing of initiation of the earliest extension. Thermochronology data (green boxes) bracket periods of rapid cooling interpreted to date normal fault–related exhumation. However, these types of data typically do not date the full duration of extension; note that in most places in the Basin and Range, most workers interpret that widespread upper-crustal extension has continued (albeit discontinuously) from the middle Miocene to the present (e.g., Dickinson, 2002, 2006; Colgan et al., 2006; Colgan and Henry, 2009). The inset on the lower right shows timing estimates for extension in the Snake Range and adjacent ranges to the north and south. Plio.—Pliocene; Quat.—Quaternary. State abbreviations: UT—Utah, NV—Nevada, CA—California.

TABLE 4. COMPILATION OF PUBLISHED EXTENSION TIMING ESTIMATES WITHIN 100 KM NORTH OR SOUTH OF THE SECTION LINE

Number on Figure 4	Location	Data source	Distance from cross section line (km)	Extension timing (Ma)	Extension magnitude*	Explanation of supporting data
1	Sanpete Valley to Juab Valley	Constenius (1996)	0–50 to S, 0–100 to N	39–27	Low	Synextensional tuffaceous rocks and sediments in half grabens in Sevier fold-and-thrust belt
2	Canyon Range	Stockli et al. (2001)	0–10 to N	19–15	High	AFT data from Cambrian quartzite; dates initiation of motion on Sevier Desert detachment
3	Mineral Mountains	Coleman et al. (1997)	80–110 to S	11 to <9	High	Field relations, geochronology, and biotite Ar/Ar geochronology
4	Drum Mountains	Lindsey (1982)	25–50 to N	21–7	Low	Bracketed between ca. 21 Ma pre-extensional and ca. 6–7 Ma postextensional volcanic rocks
5	House Range	Stockli (1999)	0–5 to S	20–15	Low	Modeling of AFT data defines ca. 20–15 Ma rapid exhumation of Jurassic granite
6	House Range	Hintze and Davis (2002)	0–20 to S, 0–20 to N	<35.4 (maximum)	Low	Volcanic rocks as young as ca. 35.4 Ma predate normal faulting
7	Confusion Range	Hintze and Davis (2002)	0–20 to N, 0–20 to S	<30.5 (maximum)	Low	Volcanic rocks as young as ca. 30.5 Ma predate normal faulting
8	Northern Deep Creek Range	Potter et al. (1995)	100–110 to N	56–39	Low	Early Eocene sedimentary rocks deformed by normal faults prior to 39 Ma volcanism
9	Deep Creek Range	Gans et al. (1991)	60–80 to N	37–34, 18–14	High	Two pulses of rapid cooling (AFT, ZFT, muscovite, biotite, and K-feldspar Ar/Ar)
10	Northern Snake Range	Gans et al. (1989)	35–50 to N	39–35	High	Field relations, K-Ar ages of pre- and synextensional volcanic rocks
11	Northern Snake Range	Miller et al. (1999b)	0–5 to S, 0–50 to N	23–12	High	Based on total range of AFT ages (dates cluster around ca. 17 Ma)
12	Northern Snake Range	Lee and Sutter (1991)	3–23 to N	37–24	High	Dates timing of cooling associated with mylonitic deformation (muscovite, biotite, and K-feldspar Ar/Ar)
13	Northern Snake Range	Lee (1995)	13–22 to N	48–41, 30–26, 20–16	High	Rapid cooling pulses interpreted as denudation timing (K-feldspar Ar/Ar diffusion domain modeling)
14	Northern Snake Range	Gébelin et al. (2015)	2–12 to N	49–45, 27–21	High	Eocene cooling on W flank of range, Miocene on E flank (muscovite Ar/Ar)
15	Northern Snake Range	Lee et al. (2017)	0–3 to S, 0–30 to N	37.8–22.5	High	U-Pb dating of deformed and undeformed rhyolite dikes: brackets timing of fabric development
16	Southern Snake Range	Miller et al. (1999b)	15–30 to S	32–16	High	Total range of AFT ages: ca. 32–20 Ma in west part of range, ca. 19–15 Ma in east part
17	Southern Snake Range	Evans et al. (2015)	15–30 to S	50–38, 33–23, 23–8	High	Modeling of AHe and ZHe ages defines three cooling pulses from Eocene to Miocene
18	Schell Creek Range	Miller et al. (1999b)	20–40 to N	22–13	High	Range of AFT ages from footwall of range-bounding fault
19	Schell Creek Range	Gans et al. (1989)	10–20 to N	36–27.4	Low	Low-offset normal faults are syn- or post–36 Ma volcanism; early extension completed before 27.4 Ma
20	Northern Egan Range	Stockli (1999)	10–100 to N	18.3–13.5	High	Range of AFT ages from eastern flank of range
21	Northern Egan Range	Gans and Miller (1983)	40–60 to N	35.8	High	Field relations imply earliest extension during 35.8 Ma volcanism
22	Central Egan Range	Gans et al. (2001)	0–10 to N	37.6–36.7	High	Bracketed with Ar/Ar ages of pre-, syn-. and postextensional volcanic rocks
23	Southern Egan Range	Drushcke et al. (2009b)	80 to S	59.2–56.0	Low	Upper Paleocene synextensional rocks coarsen toward Shingle Pass fault
24	Southern Egan Range	Druschke et al. (2009a)	60 to S	81.3–66.1	Low	Synextensional sedimentary rocks deposited in half graben formed by Ninemile fault
25	Southern White Pine Range	Stockli (1999)	60 to S	15.9–13.4	Low	Range of AFT ages from plutons near Currant
26	Northern Grant Range	Horton and Schmitt (1998)	60–80 to S	16–9	High	Synextensional deposition of Horse Camp basin
27	Central Grant Range	Long and Walker (2015)	90 to S	32–29	High	Initiation of extension postdates 32 Ma volcanics and predates 29 Ma dike
28	Southern Ruby Mountains	Colgan et al. (2010)	90–100 to N	17–10	High	Rapid cooling of Harrison Pass pluton from 17 to 10 Ma based on thermal modeling (AFT, AHe)
29	Northern Pancake Range	Nolan et al. (1974)	0–5 to S	<22.6 (maximum)	Low	Volcanic rocks as young as the 22.6 Ma Bates Mountain Tuff predate normal faulting
30	Diamond Mts./ Fish Creek Range	Long et al. (2015)	0–10 to S, 0–10 to N	75–60	High	Late Cretaceous–Paleocene cooling (ZFT, ZHe, AFT, AHe) interpreted as fault-related exhumation
31	Cortez Mountains	Colgan and Henry (2009)	90–100 to N	15.2–9	Low	Range-bounding normal fault cuts 15.2 Ma sedimentary rocks; cooling through AFT closure at 9 Ma
32	Monitor Range	Sargent and McKee (1969)	15–25 to S	<22 (maximum)	Low	Volcanic rocks as young as the 24–22 Ma Bates Mountain Tuff predate normal faulting
33	Toquima Range	Shawe et al. (1987)	40–50 to S	18–14.1	Low	Range of AFT ages that postdate cooling associated with ignimbrite flare-up volcanism
34	Toquima Range	McKee (1976)	0–10 to S, 0–10 to N	<30.1 (maximum)	Low	Volcanic rocks as young as 30.1 Ma predate normal faulting
35	Northern Toiyabe, Shoshone Ranges	Colgan et al. (2008)	110–120 to N	16–10	High	Sediments in half grabens deposited during high-magnitude extension of Caetano caldera
36	Toiyabe Range	Stockli (1999)	5–60 to N	18.4–13.3	Low	Range of AFT ages from plutons along eastern flank of range and along Highway 50
37	San Antonio Mountains	Bonham and Garside (1979)	80–100 to S	22–16	Low	Earliest normal faults postdate 22 Ma ash-flow tuffs but predate 16 Ma andesite flows
38	Royston Hills	Seedorff (1991)	50–70 to S	27–20	Low	Earliest normal faulting bracketed by pre- and postfaulting ash-flow tuffs

(*continued*)

TABLE 4. COMPILATION OF PUBLISHED EXTENSION TIMING ESTIMATES WITHIN 100 KM NORTH OR SOUTH OF THE SECTION LINE (*continued*)

Number on Figure 4	Location	Data source	Distance from cross section line (km)	Extension timing (Ma)	Extension magnitude*	Explanation of supporting data
39	Paradise Range	McKee and John (1987)	0–5 to S, 0–10 to N	16	High	Sheep Canyon fault cuts 16 Ma dike; most high-angle normal faults in range likely formed at ca. 16 Ma
40	Paradise Range	John et al. (1989)	3–5 to S	22–19	Low	Angular unconformities in 22–19 Ma volcanics indicate earliest extension
41	Cedar Mountains	Hardyman et al. (1993)	40–50 to S	27	Low	Earliest normal faulting at ca. 27 Ma, bracketed by pre- and postfaulting tuffs
42	Gillis and Gabbs Valley Ranges	Hardyman and Oldow (1991)	0–50 to S, 0–50 to N	13–8	Low	Onset of major extension and strike-slip, dated by deposition of synextensional sedimentary rocks
43	Gabbs Valley Range	Ekren et al. (1980)	0–10 to S	25	Low	Bracketing of pre- and postextensional volcanics; brackets earliest extension and strike-slip faulting
44	Southern Stillwater Range	John (1993)	70–80 to N	24–23	Low	Earliest normal faulting bracketed by pre- and postfaulting tuffs
45	Terrill Mountains	Carlson (2017)	30–50 to N	19–10	Low	Onset of major extension postdates 19 Ma volcanics; transition to mostly dextral shear by 10 Ma
46	Terrill Mountains	John et al. (1993)	30–50 to N	23–21.8	Low	Earliest extension bracketed by unconformities between pre- and postextensional volcanics
47	Wassuk Range	Stockli et al. (2002)	0–7 to S	15–12	High	Rapid exhumation from modeling of AFT and AHe ages from footwalls of domino-style normal faults
48	Northern Wassuk Range	Dilles and Gans (1995)	20–30 to N	26–22.2	Low	Earliest extension and strike-slip from bracketing of pre- and postextensional volcanics
49	Singatse Range	Dilles and Gans (1995)	0–20 to N	15.0–12.6	High	Bracketing from pre- and postextensional volcanic and intrusive units
50	Singatse Range	Surpless et al. (2002)	0–5 to S, 0–5 to N	14.1–13.6	High	Timing of rapid cooling from modeling of AFT ages
51	Pine Nut Mountains	Surpless et al. (2002)	20–25 to S	10–3	Low	Cooling history interpreted as fault-related exhumation, from modeling of AFT ages
52	Southern Virginia Mountains	Vikre et al. (1988)	20–30 to N	13–14	Low	13–14 Ma andesite and dacite contemporary with earliest normal faulting
53	Pine Nut Mountains/Carson Valley	Cashman et al. (2009)	0–30 to S	7–2	Low	Synextensional late Miocene sedimentary rocks; dates motion on Carson range-bounding fault
54	Carson Range	Surpless et al. (2002)	5–10 to N	10–3	Low	Cooling history interpreted as fault-related exhumation, from modeling of AFT ages
55	Verdi-Boca Basin	Trexler et al. (2000)	70–80 to N	12–3	Low	Timing of synextensional deposition in Verdi-Boca Basin
56	Verdi-Boca Basin	Henry and Perkins (2001)	70–80 to N	12–3	Low	Timing of synextensional deposition in Verdi-Boca Basin

Note: Abbreviations: AFT—apatite fission-track; AHe—apatite (U-Th)/He; ZFT—zircon fission-track; ZHe—zircon (U-Th)/He; Ar/Ar—$^{40}Ar/^{39}Ar$.
*"Low" extension magnitude is below 50%, and "high" extension magnitude is above 50%. This designation is approximate, as not all studied areas have quantitative estimates of extension.

Evidence for Late Cretaceous–Paleocene extension during shortening in the Sevier thrust belt is limited to domain 2, specifically to the Diamond Mountains and Fish Creek Range (Long et al., 2015) and the southern Egan Range (Druschke et al., 2009a). Synorogenic extension in the Sevier hinterland has been interpreted as a consequence of isostatic adjustment and thermal weakening following lithospheric delamination beneath eastern Nevada (Wells and Hoisch, 2008; Wells et al., 2012). Evidence for extension that postdates Sevier shortening but predates the ignimbrite flare-up is also limited to domain 2, and it includes late Paleocene extension in the southern Egan Range (Druschke et al., 2009b), early–middle Eocene extension in the Deep Creek Range (Potter et al., 1995), and ca. 50–40 Ma initial exhumation-related cooling in the Snake Range (Lee, 1995; Gébelin et al., 2015; Evans et al., 2015).

There is evidence in all four domains for extension either during or closely following the late Eocene–early Miocene sweep of ignimbrite volcanism (Henry and John, 2013). In domain 1, this consisted of normal-sense reactivation of Sevier thrust belt structures (Constenius, 1996). In domain 2, this included denudation-related cooling and formation of ductile fabrics in the Snake Range (Gans et al., 1989; Lee and Sutter, 1991; Lee, 1995; Gébelin et al., 2015; Evans et al., 2015; Lee et al., 2017), late Eocene–Oligocene synvolcanic normal faulting in the Schell Creek and Egan Ranges (Gans and Miller, 1983; Gans et al., 1989, 2001), and Oligocene extension in the Grant Range (Long and Walker, 2015). In domains 3 and 4, this included Oligocene–early Miocene (ca. 27–20 Ma), low-magnitude, synvolcanic extension in multiple localities between the Toiyabe Range and Wassuk Range (reviewed by John et al., 1989; Dilles and Gans, 1995).

All domains record evidence for widespread extension from the middle Miocene (ca. 15–17 Ma) until at least ca. 8 Ma (Fig. 4). In domain 4, all high-magnitude (>150%) extension in the Paradise, Wassuk, and Singatse Ranges was accommodated after ca. 16 Ma (John et al., 1989; Dilles and Gans, 1995; Stockli et al., 2002; Surpless et al., 2002). Much of the high-magnitude (>50%) extension in domain 2, including offset on the Sevier Desert detachment (Stockli et al., 2001), and a significant portion of the total extension in the Snake, Egan, and Schell Creek Ranges (Miller et al., 1999b; Lee, 1995; Stockli, 1999; Evans et al., 2015), occurred during the middle Miocene.

To summarize, domain 2 records a protracted transition to an extensional regime, consisting of spatially isolated extension between the Late Cretaceous and Oligocene, and the onset of widespread extension in the middle Miocene. In contrast, all of the high-magnitude extension in domain 4 took place from the middle Miocene to the present. Differences in upper-crustal rheology may, in part, explain the varying extensional histories of these two domains. The upper crust of domain 4 is dominated by a vast granitic batholith complex up to ~25–30 km thick (e.g., Ducea, 2001). In contrast, the upper crust of domain 2 contains an ~15-km-thick section of sedimentary rocks, consisting of interlayered quartzite and argillite in the lower half, and mostly carbonate and mudstone in the upper half (e.g., Stewart, 1980). This thick sedimentary section was riddled with strength anisotropies, including stratigraphic contacts between stronger and weaker lithologies, and inherited Cordilleran contractional structures including thrust faults, regional-scale folds, and the basal décollement of the Sevier thrust belt. Therefore, down to the quartz crystal-plastic transition at ~12–15 km (~300 °C at a geothermal gradient of ~20–25 °C/km; e.g., Stipp et al., 2002), the rheology of these two domains was likely quite different, with a strong, isotropic granitic batholith complex in domain 4, and an anisotropic, deformed sedimentary section in domain 2 that was relatively weak in comparison.

It has been documented that the dominant control on the location of Cenozoic extension was the spatial extent of crust thickened during Cordilleran orogenesis (e.g., Dickinson, 2002). Therefore, gradients in crustal thickness (and therefore gravitational potential energy) between the Cordilleran crust and its surroundings can be interpreted as the underlying factor that promoted extension (e.g., Dickinson, 2006; Wells and Hoisch, 2008; Colgan and Henry, 2009; Cassel et al., 2014). However, the extension timing compilation supports a scenario in which significant lateral gradients in gravitational potential energy were maintained for tens of millions of years, and punctuated geodynamic driving events were necessary to trigger major extensional episodes. Nearly all of the extension in domain 2 can be related temporally to specific geodynamic events, including isostatic and thermal adjustment of the Sevier orogenic wedge following Late Cretaceous delamination of mantle lithosphere (Wells and Hoisch, 2008; Wells et al., 2012), convective heating, volcanism, and a decrease in interplate coupling accompanying late Eocene–early Miocene slab rollback (e.g., Coney and Harms, 1984; Humphreys, 1995; Dickinson, 2002), and most importantly, the demise of Andean-type subduction and increasing influence of the San Andreas transform in the middle Miocene (Atwater, 1970; Faulds and Henry, 2008). Therefore, though gradients in gravitational potential energy were the underlying driving mechanism, geodynamic events that altered boundary conditions, including the lithospheric density column, interplate coupling, and plate-boundary configuration, were necessary to initiate pulses of gravitational collapse and caused extension to proceed in distinct episodes.

CONCLUSIONS

(1) Retrodeformation of a cross section spanning the Basin and Range Province at ~39°N yields 230 ± 42 km of extension (46% ± 8%) and an average pre-extensional crustal thickness of 54 ± 6 km.

(2) Domains of high-magnitude (~60%–66%) and low-magnitude (~11%) average extension can be defined at the scale of multiple ranges, and these correspond spatially with Cordilleran provinces that are predicted to have had high and low crustal thicknesses, respectively. Therefore, inherited variations in Cordilleran crustal thickness are interpreted as the primary control on strain distribution. The eastern high-magnitude domain (60 ± 11 km restored thickness) corresponds with the western part of the Sevier thrust belt and the spatial extent of thick, underthrusted crust. The western high-magnitude domain (66 ± 5 km restored thickness) corresponds with the eastern half of the Sierra Nevada magmatic arc.

(3) The eastern high-magnitude domain underwent a protracted, Late Cretaceous to Miocene transition to an extensional regime, while extension in the western high-magnitude domain did not start until the Miocene. This is attributed to differences in rheology between eastern Nevada, which contained an anisotropic upper crust composed of deformed sedimentary rocks, and the strong, isotropic, granitic upper crust of the magmatic arc. Nearly all extension can be related temporally to geodynamic triggering events, including Late Cretaceous lithospheric delamination and associated wedge adjustment, late Eocene–early Miocene slab rollback and accompanying volcanism, and most importantly, middle Miocene establishment of the San Andreas transform. Therefore, changes in boundary conditions were necessary to initiate distinct episodes of gravitational collapse.

ACKNOWLEDGMENTS

This paper benefited from several discussions over the past 5 yr with many outstanding geologists who work in the Basin and Range Province, including Jeffrey Lee, Chris Henry, Jim Faulds, Elizabeth Miller, Joe Colgan, Michael Wells, Wanda Taylor, Sandra Wyld, David Greene, Adolph Yonkee, Eric Christiansen, Nick Hinz, and David Rodgers. Constructive reviews by Juliet Crider and Whitney Behr greatly improved this paper.

REFERENCES CITED

Allmendinger, R.W., 1992, Fold and thrust tectonics of the western United States exclusive of the accreted terranes, *in* Burchfiel, B.C., Lipman, P.W., and Zoback, M.L., eds., The Cordilleran Orogen: Conterminous U.S.: Boulder, Colorado, Geological Society of America, Geology of North America, v. G-3, p. 583–607, https://doi.org/10.1130/DNAG-GNA-G3.583.

Allmendinger, R.W., and Royse, F., Jr., 1995, Is the Sevier Desert reflection of west-central Utah a normal fault? Comment and reply: Geology, v. 23, p. 669–670, https://doi.org/10.1130/0091-7613(1995)023<0669:ITSDRO>2.3.CO;2.

Allmendinger, R.W., Sharp, J.W., Von Tish, D., Serpa, L., Brown, L., Kaufman, S., and Oliver, J., 1983, Cenozoic and Mesozoic structure of the eastern Basin and Range Province, Utah, from COCORP seismic-reflection data: Geology, v. 11, p. 532–536, https://doi.org/10.1130/0091-7613(1983)11<532:CAMSOT>2.0.CO;2.

Allmendinger, R.W., Farmer, H., Hauser, E., Sharp, J., Von Tish, D., Oliver, J., and Kaufman, S., 1986, Phanerozoic tectonics of the Basin and Range–Colorado Plateau transition from COCORP data and geologic data: A review, *in* Barazangi, M., and Brown, L., eds., Reflection Seismology: The Continental Crust: American Geophysical Union Geodynamics Monograph 14, p. 257–267, https://doi.org/10.1029/GD014p0257.

Allmendinger, R.W., Hauge, T., Hauser, E.C., Potter, C.J., Klemperer, S.L., Nelson, D.K., Knuepfer, P., and Oliver, J., 1987, Overview of the COCORP 40°N transect, western United States: The fabric of an orogenic belt: Geological Society of America Bulletin, v. 98, p. 308–319, https://doi.org/10.1130/0016-7606(1987)98<308:OOTCNT>2.0.CO;2.

Anders, M.H., and Christie-Blick, N., 1994, Is the Sevier Desert reflection of west-central Utah a normal fault?: Geology, v. 22, p. 771–774, https://doi.org/10.1130/0091-7613(1994)022<0771:ITSDRO>2.3.CO;2.

Anders, M.H., Christie-Blick, N., and Wills, S., 1995, Is the Sevier Desert reflection of west-central Utah a normal fault?: Reply: Geology, v. 23, p. 670.

Anders, M.H., Christie-Blick, N., Wills, S., and Krueger, S.W., 2001, Rock deformation studies in the Mineral Mountains and Sevier Desert of west-central Utah: Implications for upper crustal low-angle normal faulting: Geological Society of America Bulletin, v. 113, p. 895–907, https://doi.org/10.1130/0016-7606(2001)113<0895:RDSITM>2.0.CO;2.

Anderson, E.M., 1951, The Dynamics of Faulting and Dyke Formation with Application to Britain: Edinburgh, UK, Oliver and Boyd, 206 p.

Anderson, R.E., 1971, Thin-skin distension in Tertiary rocks of southwestern Nevada: Geological Society of America Bulletin, v. 82, p. 43–58, https://doi.org/10.1130/0016-7606(1971)82[43:TSDITR]2.0.CO;2.

Anderson, R.E., Zoback, M.L., and Thompson, G.A., 1983, Implications of selected subsurface data on the structural form and evolution of some basins in the northern Basin and Range Province, Nevada and Utah: Geological Society of America Bulletin, v. 94, p. 1055–1072, https://doi.org/10.1130/0016-7606(1983)94<1055:IOSSDO>2.0.CO;2.

Armin, R.A., John, D.A., and Dohrenwend, J.C., 1983, Geologic Map of the Freel Peak 15′ Quadrangle, California and Nevada: U.S. Geological Survey Miscellaneous Investigations Series Map I-1424, scale 1:62,500, 1 sheet.

Armstrong, R.L., 1972, Low-angle (denudation) faults, hinterland of the Sevier orogenic belt, eastern Nevada and western Utah: Geological Society of America Bulletin, v. 83, p. 1729–1754, https://doi.org/10.1130/0016-7606(1972)83[1729:LDFHOT]2.0.CO;2.

Atwater, T., 1970, Implications of plate tectonics for the Cenozoic evolution of North America: Geological Society of America Bulletin, v. 81, p. 3513–3536, https://doi.org/10.1130/0016-7606(1970)81[3513:IOPTFT]2.0.CO;2.

Babaie, H.A., 1987, Paleogeographic and tectonic implications of the Golconda allochthon, southern Toiyabe Range, Nevada: Geological Society of America Bulletin, v. 99, p. 231–243, https://doi.org/10.1130/0016-7606(1987)99<231:PATIOT>2.0.CO;2.

Bartley, J.M., and Wernicke, B.P., 1984, The Snake Range décollement interpreted as a major extensional shear zone: Tectonics, v. 3, p. 647–657, https://doi.org/10.1029/TC003i006p00647.
Bentz, M.G., 1983, Progressive Structural and Stratigraphic Events Affecting the Roberts Mountains Allochthon in the Devil's Gate Area, Nevada [M.S. thesis]: Athens, Ohio, Ohio University, 222 p., 3 plates.
Best, M.G., Barr, D.L., Christiansen, E.H., Gromme, S., Deino, A.L., and Tingey, D.G., 2009, The Great Basin Altiplano during the middle Cenozoic ignimbrite flareup: Insights from volcanic rocks: International Geology Review, v. 51, p. 589–633, https://doi.org/10.1080/00206810902867690.
Bingler, E.C., 1978, Geologic Map of the Schurz Quadrangle: Nevada Bureau of Mines and Geology Map 60, scale 1:48,000, 1 sheet.
Bogen, N.L., and Schweickert, R.A., 1985, Magnitude of crustal extension across the northern Basin and Range Province: Constraints from paleomagnetism: Earth and Planetary Science Letters, v. 75, p. 93–100, https://doi.org/10.1016/0012-821X(85)90054-8.
Bonham, H.F., Jr., and Garside, L.J., 1979, Geology of the Tonopah, Lone Mountain, Klondike, and Northern Mud Lake Quadrangles, Nevada: Nevada Bureau of Mines and Geology Bulletin 92, 142 p., scale 1:48,000.
Bortz, L.C., 1959, Geology of the Copenhagen Canyon Area, Monitor Range, Eureka County, Nevada [M.S. thesis]: Reno, Nevada, University of Nevada–Reno, 56 p., 3 plates.
Brokaw, A.L., 1967, Geologic Map and Sections of the Ely Quadrangle, White Pine County, Nevada: U.S. Geological Survey Geologic Quadrangle Map GQ-697, scale 1:24,000, 1 sheet.
Brokaw, A.L., and Barosh, P.J., 1968, Geologic Map of the Riepetown Quadrangle, White Pine County, Nevada: U.S. Geological Survey Geologic Quadrangle Map GQ-758, scale 1:24,000, 1 plate.
Brokaw, A.L., and Heidrick, T., 1966, Geologic Map and Sections of the Giroux Wash Quadrangle, White Pine County, Nevada: U.S. Geological Survey Geologic Quadrangle Map I-449, scale 1:24,000, 1 sheet.
Burchfiel, B.C., and Davis, G.A., 1975, Nature and controls of Cordilleran orogenesis, western United States—Extension of an earlier synthesis: American Journal of Science, v. 275A, p. 363–396.
Camilleri, P.A., and Chamberlain, K.R., 1997, Mesozoic tectonics and metamorphism in the Pequop Mountains and Wood Hills region, northeast Nevada: Implications for the architecture and evolution of the Sevier orogen: Geological Society of America Bulletin, v. 109, p. 74–94, https://doi.org/10.1130/0016-7606(1997)109<0074:MTAMIT>2.3.CO;2.
Carlson, C.W., 2017, Kinematics and Transfer Mechanisms of Strain Accommodation at the Transition between the Northern and Central Walker Lane, Western Nevada [Ph.D. dissertation]: Reno, Nevada, University of Nevada–Reno, 220 p.
Cashman, P.H., Trexler, J.H., Jr., Muntean, T.W., Faulds, J.E., Louie, J.N., and Oppliger, G.L., 2009, Neogene tectonic evolution of the Sierra Nevada–Basin and Range transition zone at the latitude of Carson City, Nevada, *in* Oldow, J.S., and Cashman, P.H., eds., Late Cenozoic Structure and Evolution of the Great Basin–Sierra Nevada Transition: Geological Society of America Special Paper 447, p. 171–188.
Cassel, E.J., Breecker, D.O., Henry, C.D., Larson, T.E., and Stockli, D.F., 2014, Profile of a paleo-orogen: High topography across the present-day Basin and Range from 40 to 23 Ma: Geology, v. 42, p. 1007–1010, https://doi.org/10.1130/G35924.1.
Catchings, R.D., 1992, A relation among geology, tectonics, and velocity structure, western to central Basin and Range: Geological Society of America Bulletin, v. 104, p. 1178–1192, https://doi.org/10.1130/0016-7606(1992)104<1178:ARAGTA>2.3.CO;2.
Chapman, J.B., Ducea, M.N., DeCelles, P.G., and Profeta, L., 2015, Tracking changes in crustal thickness during orogenic evolution with Sr/Y: An example from the North American Cordillera: Geology, v. 43, p. 919–922, https://doi.org/10.1130/G36996.1.
Cohen, D.K., 1980, The Geology and Petrography of the Millet Ranch Plutons: A Mixed Magma [M.S. thesis]: Reno, Nevada, University of Nevada–Reno, 62 p.
Coleman, D.S., Bartley, J.M., Walker, J.D., Price, D.E., and Friedrich, A.M., 1997, Extensional faulting footwall deformation and plutonism in the Mineral Mountains, southern Sevier Desert, *in* Link, P.K., ed., Mesozoic to Recent Geology of Utah: Brigham Young University Geology Studies 42, p. 203–233.
Colgan, J.P., 2013, Reappraisal of the relationship between the northern Nevada rift and Miocene extension in the northern Basin and Range Province: Geology, v. 41, p. 211–214, https://doi.org/10.1130/G33512.1.
Colgan, J.P., and Henry, C.D., 2009, Rapid middle Miocene collapse of the Mesozoic orogenic plateau in north-central Nevada: International Geology Review, v. 51, p. 920–961, https://doi.org/10.1080/00206810903056731.
Colgan, J.P., Dumitru, T.A., Reiners, P.W., Wooden, J.L., and Miller, E.L., 2006, Cenozoic tectonic evolution of the Basin and Range Province in northwestern Nevada: American Journal of Science, v. 306, p. 616–654, https://doi.org/10.2475/08.2006.02.
Colgan, J.P., John, D.A., Henry, C.D., and Fleck, R.J., 2008, Large-magnitude Miocene extension of the Eocene Caetano caldera, Shoshone and Toiyabe Ranges, Nevada: Geosphere, v. 4, p. 107–130, https://doi.org/10.1130/GES00115.1.
Colgan, J.P., Howard, K.A., Fleck, R.J., and Wooden, J.L., 2010, Rapid middle Miocene extension and unroofing of the southern Ruby Mountains, Nevada: Tectonics, v. 29, TC6022, https://doi.org/10.1029/2009TC002655.
Coney, P.J., 1974, Structural analysis of the Snake Range décollement, east-central Nevada: Geological Society of America Bulletin, v. 85, p. 973–978, https://doi.org/10.1130/0016-7606(1974)85<973:SAOTSR>2.0.CO;2.
Coney, P.J., and Harms, T., 1984, Cordilleran metamorphic core complexes; Cenozoic extensional relics of Mesozoic compression: Geology, v. 12, p. 550–554, https://doi.org/10.1130/0091-7613(1984)12<550:CMCCCE>2.0.CO;2.
Constenius, K.N., 1996, Late Paleogene extensional collapse of the Cordilleran foreland fold and thrust belt: Geological Society of America Bulletin, v. 108, p. 20–39, https://doi.org/10.1130/0016-7606(1996)108<0020:LPECOT>2.3.CO;2.
Coogan, J.C., and DeCelles, P.G., 1996, Seismic architecture of the Sevier Desert detachment basin: Evidence for large-scale regional extension: Geology, v. 24, p. 933–936, https://doi.org/10.1130/0091-7613(1996)024<0933:ECATSD>2.3.CO;2.
Coogan, J.C., and DeCelles, P.G., 2007, Regional structure and kinematic history of the Sevier fold-and-thrust belt, central Utah: Reply: Geological Society of America Bulletin, v. 119, p. 508–512, https://doi.org/10.1130/B26176.1.
Cooper, F.J., Platt, J.P., Anczkiewicz, R., and Whitehouse, J., 2010, Footwall dip of a core complex detachment fault: Thermobarometric constraints from the northern Snake Range (Basin and Range, USA): Journal of Metamorphic Geology, v. 28, p. 997–1020, https://doi.org/10.1111/j.1525-1314.2010.00907.x.
Cowell, P.F., 1986, Structure and Stratigraphy of Part of the Northern Fish Creek Range, Eureka County, Nevada [M.S. thesis]: Corvallis, Oregon, Oregon State University, 96 p.
DeCelles, P.G., 2004, Late Jurassic to Eocene evolution of the Cordilleran thrust belt and foreland basin system, western U.S.A.: American Journal of Science, v. 304, p. 105–168, https://doi.org/10.2475/ajs.304.2.105.
DeCelles, P.G., and Coogan, J.C., 2006, Regional structure and kinematic history of the Sevier fold-and-thrust belt, central Utah: Geological Society of America Bulletin, v. 118, p. 841–864, https://doi.org/10.1130/B25759.1.
DeCelles, P.G., Lawton, T.F., and Mitra, G., 1995, Thrust timing, growth of structural culminations, and synorogenic sedimentation in the type area of the Sevier orogenic belt, central Utah: Geology, v. 23, p. 699–702, https://doi.org/10.1130/0091-7613(1995)023<0699:TTGOSC>2.3.CO;2.
DeCelles, P.G., Ducea, M.H., Kapp, P., and Zandt, G., 2009, Cyclicity in Cordilleran orogenic systems: Nature Geoscience, v. 2, p. 251–257, https://doi.org/10.1038/ngeo469.
Dickinson, W.R., 1997, Tectonic implications of Cenozoic volcanism in coastal California: Geological Society of America Bulletin, v. 109, p. 936–954, https://doi.org/10.1130/0016-7606(1997)109<0936:OTIOCV>2.3.CO;2.
Dickinson, W.R., 2000, Geodynamic interpretation of Paleozoic tectonic trends oriented oblique to the Mesozoic Klamath-Sierran continental margin in California, *in* Soreghan, M.J., and Gehrels, G.E., eds., Paleozoic and Triassic Paleogeography and Tectonics of Western Nevada and Northern California: Geological Society of America Special Paper 347, p. 209–245, https://doi.org/10.1130/0-8137-2347-7.209.
Dickinson, W.R., 2002, The Basin and Range Province as a composite extensional domain: International Geology Review, v. 44, p. 1–38, https://doi.org/10.2747/0020-6814.44.1.1.
Dickinson, W.R., 2004, Evolution of the North American Cordillera: Annual Review of Earth and Planetary Sciences, v. 32, p. 13–45, https://doi.org/10.1146/annurev.earth.32.101802.120257.
Dickinson, W.R., 2006, Geotectonic evolution of the Great Basin: Geosphere, v. 2, p. 353–368, https://doi.org/10.1130/GES00054.1.
Dickinson, W.R., and Snyder, W.S., 1978, Plate tectonics of the Laramide orogeny, *in* Matthews, V., III, ed., Laramide Folding Associated with Basement Block Faulting in the Western United States: Geological Society of America Memoir 151, p. 355–366.
Dilek, Y., and Moores, E.M., 1999, A Tibetan model for the Early Tertiary western United States: Journal of the Geological Society [London], v. 156, p. 929–941, https://doi.org/10.1144/gsjgs.156.5.0929.
Dilles, J.H., and Gans, P.B., 1995, The chronology of Cenozoic volcanism and deformation in the Yerington area, western Basin and Range and Walker Lane: Geological Society of America Bulletin, v. 107, p. 474–486, https://doi.org/10.1130/0016-7606(1995)107<0474:TCOCVA>2.3.CO;2.
Drewes, H., 1967, Geology of the Connors Pas Quadrangle, Schell Creek Range, East-Central Nevada: U.S. Geological Survey Professional Paper57, scale 1:48,000, 1 sheet, 93 p.
Druschke, P., Hanson, A.D., Wells, M.L., Rasbury, T., Stockli, D.F., and Gehrels, G., 2009a, Synconvergent surface-breaking normal faults of Late Cretaceous age within the Sevier hinterland, east-central Nevada: Geology, v. 37, p. 447–450, https://doi.org/10.1130/G25546A.1.
Druschke, P., Hanson, A.D., and Wells, M.S., 2009b, Structural, stratigraphic, and geochronologic evidence for extension predating Palaeogene volcanism in the Sevier hinterland, east-central Nevada: International Geology Review, v. 51, p. 743–775, https://doi.org/10.1080/00206810902917941.
Ducea, M., 2001, The California arc: Thick granitic batholiths, eclogitic residues, lithospheric-scale thrusting, and magmatic flare-ups: GSA Today, v. 11, no. 11, p. 4–10, https://doi.org/10.1130/1052-5173(2001)011<0004:TCATGB>2.0.CO;2.
Ducea, M.N., and Saleeby, J.B., 1998, A case for delamination of the deep batholithic crust beneath the Sierra Nevada, California: International Geology Review, v. 40, p. 78–93, https://doi.org/10.1080/00206819809465199.
Eckberg, E.E., Hitzman, M., Manydeeds, S., and Nelson, E.P., 2005, Evidence for pre–Walker Lane extension in the Copper Hill area, NW Gillis Range, Mineral County, Nevada, *in* Rhoden, H.N., Steininger, R.C., and Vikre, P.G., eds., Geological Society of Nevada Window to the World Symposium 2005: Reno, Nevada, Geological Society of Nevada, p. 315–326.
Ekren, E.B., and Byers, F.M., Jr., 1984, The Gabbs Valley Range—A well-exposed segment of the Walker Lane in west-central Nevada, *in* Lintz, J., Jr., ed., Western Geologic Excursions, Volume 4: Reno, Nevada, Geological Society of America, Annual Meeting Guidebook, p. 203–215.
Ekren, E.B., and Byers, F.M., Jr., 1986a, Geologic Map of the Mount Annie NE, Mount Annie, Ramsay Spring,

and Mount Annie SE Quadrangles, Mineral and Nye Counties, Nevada: U.S. Geological Survey Miscellaneous Investigations Series Map I-1579, 1 sheet, scale 1:48,000.

Ekren, E.B., and Byers, F.M., Jr., 1986b, Geologic Map of the Murphys Well, Pilot Cone, Copper Mountain, and Poinsettia Spring Quadrangles, Mineral and Nye Counties, Nevada: U.S. Geological Survey Miscellaneous Investigations Series Map I-1576, 1 sheet, scale 1:48,000.

Ekren, E.B., Byers, F.M., Jr., Hardyman, R.F., Marvin, R.F., and Silberman, M.L., 1980, Stratigraphy, preliminary petrology, and Some Structural Features of Tertiary Volcanic Rocks in the Gabbs Valley and Gillis Ranges, Mineral County, Nevada: U.S. Geological Survey Bulletin 1464, 54 p.

Elliott, D., 1983, The construction of balanced cross-sections: Journal of Structural Geology, v. 5, p. 101, https://doi.org/10.1016/0191-8141(83)90035-4.

Evans, S.L., Styron, R.H., van Soest, M.C., Hodges, K.V., and Hanson, A.D., 2015, Zircon and apatite (U-Th)/He evidence for Paleogene and Neogene extension in the Southern Snake Range, Nevada, USA: Tectonics, v. 34, p. 2142–2164, https://doi.org/10.1002/2015TC003913.

Evenchick, C.A., McMechan, M.E., McNicoll, V.J., and Carr, S.D., 2007, A synthesis of the Jurassic–Cretaceous tectonic evolution of the central and southeastern Canadian Cordillera: Exploring links across the orogen, *in* Sears, J.W., Harms, T.A., and Evenchick, C.A., eds., Whence the Mountains? Inquiries into the Evolution of Orogenic Systems: A Volume in Honor or Raymond A. Price: Geological Society of America Special Paper 433, p. 117–145, https://doi.org/10.1130/2007.2433(06).

Faulds, J.E., and Henry, C.D., 2008, Tectonic influences on the spatial and temporal evolution of the Walker Lane: An incipient transform fault along the evolving Pacific–North American plate boundary, *in* Spencer, J.E., and Titley, S.R., eds., Ores and Orogenesis: Circum-Pacific Tectonics, Geologic Evolution, and Ore Deposits: Tucson, Arizona Geological Society Digest Volume 22, p. 437–470.

Faulds, J.E., and Stewart, J.H., eds., 1998, Accommodation Zones and Transfer Zones: The Regional Segmentation of the Basin and Range Province: Geological Society of America Special Paper 323, 257 p.

Ferguson, H.G., and Cathcart, S.H., 1954, Geologic Map of the Round Mountain Quadrangle, Nevada: U.S. Geological Survey Geologic Quadrangle Map 40, scale 1:125,000, 1 sheet.

Fouch, T.D., Hanley, J.M., and Forester, R.M., 1979, Preliminary correlation of Cretaceous and Paleogene lacustrine and related nonmarine sedimentary and volcanic rocks in parts of the Great Basin of Nevada and Utah, *in* Newman, G.W., and Goode, H.D., eds., Basin and Range Symposium and Great Basin Field Conference: Denver, Rocky Mountain Association of Petroleum Geologists and Utah Geological Association, p. 305–312.

Frei, I.S., Magill, J.R., and Cox, A., 1984, Paleomagnetic results from the central Sierra Nevada: Constraints on reconstructions of the western United States: Tectonics, v. 3, p. 157–177, https://doi.org/10.1029/TC003i002p00157.

French, D.E., 1993, Thrust faults in the southern Diamond Mountains, Eureka and White Pine Counties, Nevada, *in* Gillespie, C.W., ed., Structural and Stratigraphic Relationships of Devonian Reservoir Rocks, East-Central Nevada: Reno, Nevada Petroleum Society, 1993 Field Conference Guidebook NPS 07, p. 105–114.

Gans, P.B., 1987, An open-system, two-layer crustal stretching model for the eastern Great Basin: Tectonics, v. 6, p. 1–12, https://doi.org/10.1029/TC006i001p00001.

Gans, P.B., and Miller, E.L., 1983, Style of mid-Tertiary extension in east-central Nevada, *in* Gurgel, K.D., ed., Geologic Excursions in the Overthrust Belt and Metamorphic Core Complexes of the Intermountain Region: Utah Geological and Mineral Survey Special Studies 59, p. 107–160.

Gans, P.B., Miller, E.L., McCarthy, J., and Oldcott, M.L., 1985, Tertiary extensional faulting and evolving ductile-brittle transition zones in the northern Snake Range and vicinity: New insights from seismic data: Geology, v. 13, p. 189–193, https://doi.org/10.1130/0091-7613(1985)13<189:TEFAED>2.0.CO;2.

Gans, P.B., Mahood, G.A., and Schermer, E., 1989, Synextensional Magmatism in the Basin and Range Province: A Case Study from the Eastern Great Basin: Geological Society of America Special Paper 223, 53 p.

Gans, P.B., Miller, E.L., Brown, R., Houseman, G., and Lister, G.S., 1991, Assessing the amount, rate and timing of tilting in normal fault blocks: A case study of tilted granites in the Kern–Deep Creek Mountains, Utah: Geological Society of America Abstracts with Programs, v. 23, no. 2, p. 28.

Gans, P.B., Seedorff, E., Fahey, P.L., Hasler, R.W., Maher, D.J., Jeanne, R.A., and Shaver, S.A., 2001, Rapid Eocene extension in the Robinson district, White Pine County, Nevada: Constraints for $^{40}Ar/^{39}Ar$ dating: Geology, v. 29, p. 475–487, https://doi.org/10.1130/0091-7613(2001)029<0475:REEITR>2.0.CO;2.

Gébelin, A., Teyssier, C., Heizler, M., and Mulch, A., 2015, Meteoric water circulation in a rolling-hinge detachment system (northern Snake Range core complex, Nevada): Geological Society of America Bulletin, v. 127, p. 149–161, https://doi.org/10.1130/B31063.1.

Gilbert, H., 2012, Crustal structure and signatures of recent tectonism as influenced by ancient terranes in the western United States: Geosphere, v. 8, p. 141–157, https://doi.org/10.1130/GES00720.1.

Greene, D.C., 2014, The Confusion Range, west-central Utah: Fold-thrust deformation and a western Utah thrust belt in the Sevier hinterland: Geosphere, v. 10, p. 148–169, https://doi.org/10.1130/GES00972.1.

Hardyman, R.F., 1980, Geologic Map of the Gillis Canyon Quadrangle, Mineral County, Nevada: U.S. Geological Survey Miscellaneous Investigations Series Map I-1237, 1 sheet, scale 1:48,000.

Hardyman, R.F., 1984, Strike-slip, normal, and detachment faults in the northern Gillis Range, Walker Lane of west central Nevada, *in* Lintz, J., Jr., ed., Western Geologic Excursions, Volume 4: Reno, Nevada, Geological Society of America, Annual Meeting Guidebook, p. 184–203.

Hardyman, R.F., and Oldow, J.S., 1991, Tertiary tectonic framework and Cenozoic history of the central Walker Lane, Nevada, *in* Raines, G.L., Lisle, R.E., Schafer, R.W., and Wilkinson, W.H., eds., Geology and Ore Deposits of the Great Basin: Symposium Proceedings Volume 1: Reno, Geological Society of Nevada, p. 279–301.

Hardyman, R.F., McKee, E.H., Snee, L.W., and Whitebread, D.H., 1993, The Camp Terrill and Dicalite Summit faults: Two contrasting examples of detachment faults in the central Walker Lane, *in* Craig, S.D., ed., Structure, Tectonics and Mineralization of the Walker Lane: Walker Lane Symposium Proceedings: Reno, Geological Society of Nevada, p. 93–113.

Harris, H.D., 1959, A late Mesozoic positive area in western Utah: American Association of Petroleum Geologists Bulletin, v. 43, p. 2636–2652.

Henry, C.D., and John, D.A., 2013, Magmatism, ash-flow tuffs, and calderas of the ignimbrite flareup in the western Nevada volcanic field, Great Basin, USA: Geosphere, v. 9, p. 951–1008, https://doi.org/10.1130/GES00867.1.

Henry, C.D., and Perkins, M.E., 2001, Sierra Nevada–Basin and Range transition near Reno, Nevada: Two-stage development at 12 and 3 Ma: Geology, v. 29, no. 8, p. 719–722, https://doi.org/10.1130/0091-7613(2001)029<0719:SNBART>2.0.CO;2.

Henry, C.D., McGrew, A.J., Colgan, J.P., Snoke, A.W., and Brueseke, M.E., 2011, Timing, distribution, amount, and style of Cenozoic extension in the northern Great Basin, *in* Lee, J., and Evans, J.P., eds., Geologic Field Trips to the Basin and Range, Rocky Mountains, Snake River Plain, and Terranes of the U.S. Cordillera: Geological Society of America Field Guide 21, p. 27–66, https://doi.org/10.1130/2011.0021(02).

Hess, R.H., Fitch, S.P., and Warren, S.N., 2004, Nevada Oil and Gas Well Database: Nevada Bureau of Mines and Geology Open-File Report 04-1, 1 p.

Hintze, L.F., 1974a, Preliminary Geologic Map of the Conger Mountain Quadrangle, Millard County, Utah: U.S. Geological Survey Miscellaneous Field Studies Map MF-634, scale 1:48,000, 2 sheets.

Hintze, L.F., 1974b, Preliminary Geologic Map of the Notch Peak Quadrangle, Millard County, Utah: U.S. Geological Survey Miscellaneous Field Studies Map MF-636, scale 1:48,000, 2 sheets.

Hintze, L.F., and Davis, F.D., 2002, Geologic Map of the Tule Valley 30′ ×60′ Quadrangle and Parts of the Ely, Fish Springs, and Kern Mountains 30′ ×60′ Quadrangles, Northwest Millard County, Utah: Utah Geological Survey Map 186, scale 1:100,000.

Hintze, L.F., and Davis, F.D., 2003, Geology of Millard County, Utah: Utah Geological Survey Bulletin 133, 305 p.

Hodges, K.V., and Walker, J.D., 1992, Extension in the Cretaceous Sevier orogen, North American Cordillera: Geological Society of America Bulletin, v. 104, p. 560–569, https://doi.org/10.1130/0016-7606(1992)104<0560:EITCSO>2.3.CO;2.

Horton, B.K., and Schmitt, J.G., 1998, Development and exhumation of a Neogene sedimentary basin during extension, east-central Nevada: Geological Society of America Bulletin, v. 110, p. 163–172, https://doi.org/10.1130/0016-7606(1998)110<0163:DAEOAN>2.3.CO;2.

Horton, T.W., Sjostrom, D.J., Abruzzese, M.J., Poage, M.A., Waldbauer, J.R., Hren, M., Wooden, J., and Chamberlain, C.P., 2004, Spatial and temporal variation of Cenozoic surface elevation in the Great Basin and Sierra Nevada: American Journal of Science, v. 304, p. 862–888, https://doi.org/10.2475/ajs.304.10.862.

Hose, R.K., 1965, Geologic Map and Sections of the Conger Range NE Quadrangle and Adjacent Area, Confusion Range, Millard County, Utah: U.S. Geological Survey Miscellaneous Geologic Investigations Map I-436, scale 1:24,000, 1 sheet.

Hose, R.K., 1977, Structural Geology of the Confusion Range, West-Central Utah: U.S. Geological Survey Professional Paper 971, p. 97–131.

Hose, R.K., and Blake, M.C., Jr., 1976, Geologic Map of White Pine County, Nevada, *in* Geology and Mineral Resources of White Pine County, Nevada: Nevada Bureau of Mines and Geology Bulletin 85, scale 1:250,000, 32 p.

Humphrey, F.L., 1960, Geologic Map of the White Pine Mining District, White Pine County, Nevada: Nevada Bureau of Mines Bulletin 57, scale 1:48,000, 119 p.

Humphreys, E.D., 1995, Post-Laramide removal of the Farallon slab, western United States: Geology, v. 23, p. 987–990, https://doi.org/10.1130/0091-7613(1995)023<0987:PLROTF>2.3.CO;2.

John, D.A., 1988, Geologic Map of Oligocene and Miocene Volcanic Rocks, Paradise Peak and Western Part of the Ione Quadrangles, Nye County, Nevada: U.S. Geological Survey Miscellaneous Field Studies Map MF-2025, scale 1:24,000, 2 sheets.

John, D.A., 1993, Late Cenozoic volcanotectonic evolution of the southern Stillwater Range, west-central Nevada, *in* Craig, S.D., ed., Structure, Tectonics and Mineralization of the Walker Lane: Walker Lane Symposium Proceedings: Reno, Geological Society of Nevada, p. 64–93.

John, D.A., Thomason, R.E., and McKee, E.H., 1989, Geology and K-Ar geochronology of the Paradise Peak Mine and the relationship of pre–Basin and Range extension to early Miocene precious metal mineralization in west-central Nevada: Economic Geology and the Bulletin of the Society of Economic Geologists, v. 84, p. 631–649, https://doi.org/10.2113/gsecongeo.84.3.631.

John, D.A., Dilles, J.H., and Hardyman, R.F., 1993, Evolution of Cenozoic magmatism and tectonism along a northeast-southwest transect across the northern Walker Lane, west-central Nevada. Road log to the southern Stillwater Range, Terrill Mountains, and northern Wassuk Range—Part II, *in* Lahren, M.M., Trexler, J.H., Jr., and Spinosa, C., eds., Crustal Evolution of the Great Basin and Sierra Nevada: Reno, Nevada, Cordilleran/Rocky Mountain Section, Geological Society America, p. 428–452.

Johnston, S.M., 2000, Normal Faulting in the Upper Plate of a Metamorphic Core Complex, Northern Snake Range,

Nevada [M.S. thesis]: Palo Alto, California, Stanford University, 60 p.
Kleinhampl, F.J., and Ziony, J.L., 1985, Geology of Northern Nye County, Nevada: Nevada Bureau of Mines and Geology Bulletin 99A, 171 p.
Lee, J., 1995, Rapid uplift and rotation of mylonitic rocks from beneath a detachment fault: Insights from potassium feldspar ^{40}Ar/^{39}Ar thermochronology, northern Snake Range, Nevada: Tectonics, v. 14, p. 54–77, https://doi.org/10.1029/94TC01508.
Lee, J., and Sutter, J.F., 1991, Incremental ^{40}Ar/^{39}Ar thermochronology of mylonitic rocks from the northern Snake Range, Nevada: Tectonics, v. 10, p. 77–100, https://doi.org/10.1029/90TC01931.
Lee, J., Miller, E.L., and Sutter, J.F., 1987, Ductile strain and metamorphism in an extensional tectonic setting: A case study from the northern Snake Range, Nevada, U.S.A., *in* Coward, M.P., Dewey, J.F., and Hancock, P.L., eds., Continental Extensional Tectonics: Geological Society, London, Special Publication 28, p. 267–298, https://doi.org/10.1144/GSL.SP.1987.028.01.18.
Lee, J., Blackburn, T., and Johnston, S., 2017, Timing of mid-crustal ductile extension in the northern Snake Range metamorphic core complex, Nevada: Evidence from U/Pb zircon ages: Geosphere, v. 13, p. 439–459, https://doi.org/10.1130/GES01429.1.
Lewis, C.J., Wernicke, B.P., Selverstone, J., and Bartley, J.M., 1999, Deep burial of the footwall of the northern Snake Range décollement, Nevada: Geological Society of America Bulletin, v. 111, p. 39–51, https://doi.org/10.1130/0016-7606(1999)111<0039:DBOTFO>2.3.CO;2.
Lindsey, D.A., 1982, Tertiary Volcanic Rocks and Uranium in the Thomas Range and Northern Drum Mountains, Juab County, Utah: U.S. Geological Survey Professional Paper 1221, 71 p.
Lohr, L.S., 1965, Geology of the Brock Canyon Area, Monitor Range, Eureka County, Nevada [M.S. thesis]: Reno, Nevada, University of Nevada–Reno, 44 p., 2 plates.
Long, S.P., 2012, Magnitudes and spatial patterns of erosional exhumation in the Sevier hinterland, eastern Nevada and western Utah, USA: Insights from a Paleogene paleogeologic map: Geosphere, v. 8, p. 881–901, https://doi.org/10.1130/GES00783.1.
Long, S.P., 2015, An upper-crustal fold province in the hinterland of the Sevier orogenic belt, eastern Nevada, U.S.A.: A Cordilleran valley and ridge in the Basin and Range: Geosphere, v. 11, p. 404–424, https://doi.org/10.1130/GES01102.1.
Long, S.P., and Walker, J.P., 2015, Geometry and kinematics of the Grant Range brittle detachment system, eastern Nevada, U.S.A.: An end-member style of upper-crustal extension: Tectonics, v. 34, p. 1837–1862, https://doi.org/10.1002/2015TC003918.
Long, S.P., Henry, C.D., Muntean, J.L., Edmondo, G.P., and Cassel, E.J., 2014a, Early Cretaceous construction of a structural culmination, Eureka, Nevada, U.S.A.: Implications for out-of-sequence deformation in the Sevier hinterland: Geosphere, v. 10, p. 564–584, https://doi.org/10.1130/GES00997.1.
Long, S.P., Henry, C.D., Muntean, J.L., Edmondo, G.P., and Thomas, R.D., 2014b, Geologic Map of the Southern Part of the Eureka Mining District, and Surrounding Areas of the Fish Creek Range, Mountain Boy Range, and Diamond Mountains, Eureka and White Pine Counties, Nevada: Nevada Bureau of Mines and Geology Map 183, scale 1:24,000, 2 plates, 36 p.
Long, S.P., Thomson, S.N., Reiners, P.W., and Di Fiori, R.V., 2015, Synorogenic extension localized by upper-crustal thickening: An example from the Late Cretaceous Nevadaplano: Geology, v. 43, p. 351–354, https://doi.org/10.1130/G36431.1.
Loomis, A.A., 1983, Geology of the Fallen Leaf Lake 15′ Quadrangle, El Dorado County, California: California Division of Mines and Geology Map Sheet 32, scale 1:62,500, 2 sheets.
McGrew, A.J., Peters, M.T., and Wright, J.E., 2000, Thermobarometric constraints on the tectonothermal evolution of the East Humboldt Range metamorphic core complex, Nevada: Geological Society of America Bulletin, v. 112, p. 45–60, https://doi.org/10.1130/0016-7606(2000)112<45:TCOTTE>2.0.CO;2.
McKee, E.H., 1976, Geology of the Northern Part of the Toquima Range, Lander, Eureka, and Nye Counties, Nevada: U.S. Geological Survey Professional Paper 931, 49 p., 2 plates.
McKee, E.H., and John, D.A., 1987, Sample Locality Map and Potassium-Argon Ages and Data for Cenozoic Igneous Rocks of the Tonopah 1° × 2° Quadrangle, Central Nevada: U.S. Geological Survey Miscellaneous Field Studies Map MF-1877-I, scale 1:250,000.
McQuarrie, N., and Wernicke, B.P., 2005, An animated tectonic reconstruction of southwestern North America since 36 Ma: Geosphere, v. 1, p. 147–172, https://doi.org/10.1130/GES00016.1.
Miller, E.L., and Gans, P.B., 1999, Geologic Map of the Cove Quadrangle, Nevada and Utah: Nevada Bureau of Mines and Geology Field Studies Map 22, scale 1:24,000, 1 sheet, 12 p.
Miller, E.L., Gans, P.B., and Garing, J., 1983, The Snake Range décollement: An exhumed mid-Tertiary ductile-brittle transition: Tectonics, v. 2, p. 239–263, https://doi.org/10.1029/TC002i003p00239.
Miller, E.L., Gans, P.B., Grier, S.P., Huggins, C.C., and Lee, J., 1999a, Geologic Map of the Old Man's Canyon Quadrangle, Nevada: Nevada Bureau of Mines and Geology Field Studies Map 21, scale 1:24,000, 1 sheet, 12 p.
Miller, E.L., Dumitru, T.A., Brown, R.W., and Gans, P.B., 1999b, Rapid Miocene slip on the Snake Range–Deep Creek Range fault system, east-central Nevada: Geological Society of America Bulletin, v. 111, p. 886–905, https://doi.org/10.1130/0016-7606(1999)111<0886:RMSOTS>2.3.CO;2.
Molnar, P., and Lyon-Caen, H., 1988, Some simple aspects of the support, structure and evolution of mountain belts, *in* Clark, S.P., Jr., Burchfiel, B.C., and Suppe, J., eds., Processes in Continental Lithosphere Deformation: Geological Society of America Special Paper 218, p. 179–207, https://doi.org/10.1130/SPE218-p179.
Nolan, T.B., Merriam, C.W., and Blake, M.C., Jr., 1974, Geologic Map of the Pinto Summit Quadrangle, Eureka and White Pine Counties, Nevada: U.S. Geological Survey Miscellaneous Investigations Series Map I-793, scale 1:31,680, 14 p., 2 plates.
Oldow, J.S., 1984, Evolution of a late Mesozoic back-arc fold and thrust belt, northwestern Great Basin, U.S.A.: Tectonophysics, v. 102, p. 245–274, https://doi.org/10.1016/0040-1951(84)90016-7.
Poole, F.G., Stewart, J.H., Palmer, A.R., Sandberg, C.A., Madrid, R.J., Ross, R.J., Jr., Hintze, L.F., Miller, M.M., and Wricke, C.T., 1992, Latest Precambrian to latest Devonian time; development of a continental margin, *in* Burchfiel, B.C., Lipman, P.W., and Zoback, M.L., eds., The Cordilleran Orogen: Conterminous U.S.: Boulder, Colorado, Geological Society of America, The Geology of North America, v. G-3, p. 9–56, https://doi.org/10.1130/DNAG-GNA-G3.9.
Potter, C.J., Dubiel, R.F., Snee, L.W., and Good, S.C., 1995, Eocene extension of early Eocene lacustrine strata in a complexly deformed Sevier-Laramide hinterland, northwest Utah and northeast Nevada: Geology, v. 23, p. 181–184, https://doi.org/10.1130/0091-7613(1995)023<0181:EEOEEL>2.3.CO;2.
Price, R.A., 1981, The Cordilleran foreland thrust and fold belt in the southern Canadian Rocky Mountains, *in* McClay, K.R., and Price, N.J., eds., Thrust and Nappe Tectonics: Geological Society, London, Special Publication 9, p. 427–448, https://doi.org/10.1144/GSL.SP.1981.009.01.39.
Proffett, J.M., Jr., 1977, Cenozoic geology of the Yerington district, Nevada, and implications for the nature and origin of Basin and Range faulting: Geological Society of America Bulletin, v. 88, p. 247–266, https://doi.org/10.1130/0016-7606(1977)88<247:CGOTYD>2.0.CO;2.
Proffett, J.M., Jr., and Dilles, J.H., 1984, Geologic Map of the Yerington District, Nevada: Nevada Bureau of Mines and Geology Map 77, scale 1:24,000, 1 sheet.
Roberts, R.J., Montgomery, K.M., and Lehner, R.E., 1967, Geology and Mineral Resources of Eureka County, Nevada: Nevada Bureau of Mines and Geology Bulletin 64, 152 p., 11 plates.
Saleeby, J., Ducea, M., and Clemens-Knott, D., 2003, Production and loss of high density batholithic root, southern Sierra Nevada, California: Tectonics, v. 22, 1064, https://doi.org/10.1029/2002TC001374.
Sargent, K.A., and McKee, E.H., 1969, The Bates Mountain Tuff in Northern Nye County, Nevada: Contributions to Stratigraphy: U.S. Geological Survey Bulletin 1294, Chapter E, 12 p.
Schalla, R.A., 1978, Paleozoic Stratigraphy of the Southern Mahogany Hills, Eureka County, Nevada [M.S. thesis]: Corvallis, Oregon, Oregon State University, 118 p., 6 plates.
Seedorff, C.E., 1991, Royston district, western Nevada—A Mesozoic porphyry copper system that was tilted and dismembered by Tertiary normal faults, *in* Raines, G.L., Lisle, R.E., Schafer, R.W., and Wilkinson, W.H., eds., Geology and Ore Deposits of the Great Basin: Symposium Proceedings: Reno, Geological Society of Nevada, p. 359–391.
Shawe, D.R., Naeser, C.W., Marvin, R.F., and Mehnert, H.H., 1987, New radiometric ages of igneous and mineralized rocks, southern Toquima Range, Nye County, Nevada: Isochron-West, v. 50, p. 3–7.
Silberling, N.J., and John, D.A., 1989, Geologic Map of Pre-Tertiary Rocks of the Paradise Range and Southern Lodi Hills, West-Central Nevada: U.S. Geological Survey Miscellaneous Field Studies Map MF-2062, scale 1:24,000, 1 sheet.
Smith, D.L., 1992, History and kinematics of Cenozoic extension in the northern Toiyabe Range, Lander County, Nevada: Geological Society of America Bulletin, v. 104, p. 789–801, https://doi.org/10.1130/0016-7606(1992)104<0789:HAKOCE>2.3.CO;2.
Smith, D.L., Gans, P.B., and Miller, E.L., 1991, Palinspastic restoration of Cenozoic extension in the central and eastern Basin and Range Province at latitude 39–40°N, *in* Raines, G.L., Lisle, R.E., Schafer, R.W., and Wilkinson, W.H., eds., Geology and Ore Deposits of the Great Basin: Symposium Proceedings: Reno, Nevada, Geological Society of Nevada, p. 75–86.
Snell, K.E., Koch, P.L., Druschke, P., Foreman, B.Z., and Eiler, J.M., 2014, High elevation of the 'Nevadaplano' during the Late Cretaceous: Earth and Planetary Science Letters, v. 386, p. 52–63, https://doi.org/10.1016/j.epsl.2013.10.046.
Snow, J.K., and Wernicke, B.P., 2000, Cenozoic tectonism in the central Basin and Range: Magnitude, rate and distribution of upper crustal strain: American Journal of Science, v. 300, p. 659–719, https://doi.org/10.2475/ajs.300.9.659.
Sonder, L.J., and Jones, C.H., 1999, Western United States extension: How the West was widened: Annual Review of Earth and Planetary Sciences, v. 27, p. 417–462, https://doi.org/10.1146/annurev.earth.27.1.417.
Speed, R.C., 1983, Evolution of the sialic margin in the central-western United States, *in* Watkins, J.S., and Drake, C.L., eds., Studies in Continental Margin Geology: American Association of Petroleum Geologists Memoir 34, p. 457–468.
Speed, R.C., and Sleep, N., 1982, Antler orogeny and foreland basin: A model: Geological Society of America Bulletin, v. 93, p. 815–828, https://doi.org/10.1130/0016-7606(1982)93<815:AOAFBA>2.0.CO;2.
Speed, R.C., Elison, M.W., and Heck, F.R., 1988, Phanerozoic tectonic evolution of the Great Basin, *in* Ernst, G., ed., Metamorphism and Crustal Evolution of the Western United States, Rubey Series Volume 7: Englewood Cliffs, New Jersey, Prentice-Hall, p. 572–605.
Stewart, J.H., 1971, Basin and Range structure—A system of horsts and grabens produced by deep-seated extension: Geological Society of America Bulletin, v. 82, p. 1019–1043, https://doi.org/10.1130/0016-7606(1971)82[1019:BARSAS]2.0.CO;2.
Stewart, J.H., 1980, Geology of Nevada: A Discussion to Accompany the Geologic Map of Nevada: Nevada Bureau of Mines and Geology Special Publication 4, 136 p.
Stewart, J.H., 1999, Geologic Map of the Carson City 30 × 60 Minute Quadrangle, Nevada: Nevada Bureau of Mines and Geology Map 118, scale 1:100,000, 1 sheet.
Stewart, J.H., and Carlson, J.E., 1978, Geologic Map of Nevada: Reston, U.S. Geological Survey in collaboration with Nevada Bureau of Mines and Geology, scale 1:500,000, 1 sheet.

Stewart, J.H., and Dohrenwend, J.C., 1984, Geologic Map of the Yerington Quadrangle, Nevada: U.S. Geological Survey Open-File Report OF-84-212, scale 1:62,500, 1 sheet.

Stewart, J.H., and Poole, F.G., 1974, Lower Paleozoic and uppermost Precambrian Cordilleran miogeocline, Great Basin, western United States, *in* Dickinson, W.R., ed., Tectonics and Sedimentation: Society of Economic Paleontologists and Mineralogists (SEPM) Special Publication 22, p. 28–57, https://doi.org/10.2110/pec.74.22.0028.

Stipp, M., Stunitz, H., Heilbronner, R., and Schmid, S.M., 2002, The eastern Tonale fault zone: A 'natural laboratory' for crystal plastic deformation over a temperature range from 250° to 700°C: Journal of Structural Geology, v. 24, p. 1861–1884, https://doi.org/10.1016/S0191-8141(02)00035-4.

Stockli, D.F., 1999, Regional Timing and Spatial Distribution of Miocene Extension in the Northern Basin and Range Province [Ph.D. thesis]: Palo Alto, California, Stanford University, 239 p.

Stockli, D.F., Linn, J.K., Walker, J.D., and Dumitru, T.A., 2001, Miocene unroofing of the Canyon Range during extension along the Sevier Desert detachment, west central Utah: Tectonics, v. 20, p. 289–307, https://doi.org/10.1029/2000TC001237.

Stockli, D.F., Surpless, B.E., Dumitru, T.A., and Farley, K.A., 2002, Thermochronological constraints on the timing and magnitude of Miocene and Pliocene extension in the central Wassuk Range, western Nevada: Tectonics, v. 21, p. 10-1–10-19, https://doi.org/10.1029/2001TC001295.

Suppe, J., 1983, Geometry and kinematics of fault-bend folding: American Journal of Science, v. 283, p. 684–721, https://doi.org/10.2475/ajs.283.7.684.

Surpless, B.E., 2012, Cenozoic tectonic evolution of the central Wassuk Range, western Nevada, USA: International Geology Review, v. 54, p. 547–571, https://doi.org/10.1080/00206814.2010.548117.

Surpless, B.E., Stockli, D.F., Dumitru, T.A., and Miller, E.L., 2002, Two-phase westward encroachment of Basin and Range extension into the northern Sierra Nevada: Tectonics, v. 21, no. 1, https://doi.org/10.1029/2000TC001257.

Taylor, W.J., Bartley, J.M., Martin, M.W., Geissman, J.W., Walker, J.D., Armstrong, P.A., and Fryxell, J.E., 2000, Relations between hinterland and foreland shortening: Sevier orogeny, central North American Cordillera: Tectonics, v. 19, no. 6, p. 1124–1143, https://doi.org/10.1029/1999TC001141.

Trexler, J.H., Cashman, P.H., Henry, C.D., Muntean, T., Schwartz, K., TenBrink, A., Faulds, J.E., Perkins, M., and Kelly, T., 2000, Neogene basins in western Nevada document the tectonic history of the Sierra Nevada–Basin and Range transition zone for the last 12 Ma, *in* Lageson, D.R., Peters, S.G., and Lahren, M.M., eds., Great Basin and Sierra Nevada: Colorado, Geological Society of America Field Guide 2, p. 97–116, https://doi.org/10.1130/0-8137-0002-7.97.

Tripp, E.C., 1957, The Geology of the North Half of the Pancake Summit Quadrangle, Nevada [M.A. thesis]: Los Angeles, California, University of Southern California, 2 plates, 87 p.

Utah Department of Natural Resources, 2017, Division of Oil, Gas, and Mining, Data Research Center, Well Files Database: https://oilgas.ogm.utah.gov/oilgasweb/live-data-search/lds-well/well-lu.xhtml (accessed 16 August 2017).

Vikre, P.G., McKee, E.H., and Silberman, M.L., 1988, Chronology of Miocene hydrothermal and igneous events in the western Virginia Range, Washoe, Storey, and Lyon Counties, Nevada: Economic Geology and the Bulletin of the Society of Economic Geologists, v. 83, p. 864–874, https://doi.org/10.2113/gsecongeo.83.4.864.

Villien, A., and Kligfield, R.M., 1986, Thrusting and synorogenic sedimentation in central Utah, *in* Peterson, J.A., ed., Paleotectonics and Sedimentation in the Rocky Mountain Region, United States: American Association of Petroleum Geologists Memoir 41, p. 281–308.

Wells, M.L., and Hoisch, T.D., 2008, The role of mantle delamination in widespread Late Cretaceous extension and magmatism in the Cordilleran orogen, western United States: Geological Society of America Bulletin, v. 120, p. 515–530, https://doi.org/10.1130/B26006.1.

Wells, M.L., Hoisch, T.D., Cruz-Aribe, A.M., and Vervoort, J.D., 2012, Geodynamics of synconvergent extension and tectonic mode switching: Constraints from the Sevier-Laramide orogeny: Tectonics, v. 31, TC1002, https://doi.org/10.1029/2011TC002913.

Wernicke, B., 1981, Low-angle normal faults in the Basin and Range Province: Nappe tectonics in an extending orogen: Nature, v. 291, p. 645–648, https://doi.org/10.1038/291645a0.

Wernicke, B., and Burchfiel, B.C., 1982, Modes of extensional tectonics: Journal of Structural Geology, v. 4, p. 105–115, https://doi.org/10.1016/0191-8141(82)90021-9.

Wernicke, B., Axen, G.J., and Snow, J.K., 1988, Basin and Range extensional tectonics at the latitude of Las Vegas, Nevada: Geological Society of America Bulletin, v. 100, p. 1738–1757, https://doi.org/10.1130/0016-7606(1988)100<1738:BARETA>2.3.CO;2.

Whitebread, D.H., Silberling, N.J., Brem, G.F., and Andrews, T.D., 1988, Preliminary Geologic Map of the Eastern Half of the Ione Quadrangle, Nye County, Nevada: U.S. Geological Survey Open-File Report 88-48, scale 1:62,500, 1 sheet.

Wolfe, J., Schorn, H., Forest, C., and Molnar, P., 1997, Paleobotanical evidence for high altitudes in Nevada during the Miocene: Science, v. 276, p. 1672–1675, https://doi.org/10.1126/science.276.5319.1672.

Wright, L.A., and Troxel, B.W., 1973, Shallow-fault interpretation of Basin and Range structure, southwestern Great Basin, *in* de Jong, K.A., and Scholten, R., eds., Gravity and Tectonics: New York, John Wiley and Sons, p. 397–407.

Wyld, S.J., 2002, Structural evolution of a Mesozoic backarc fold-and-thrust belt in the U.S. Cordillera: New evidence from northern Nevada: Geological Society of America Bulletin, v. 114, p. 1452–1468, https://doi.org/10.1130/0016-7606(2002)114<1452:SEOAMB>2.0.CO;2.

Wyld, S.J., Rogers, J.W., and Copeland, P., 2003, Metamorphic evolution of the Luning-Fencemaker fold-thrust belt, Nevada: Illite crystallinity, metamorphic petrology, and ^{40}Ar/^{39}Ar geochronology: The Journal of Geology, v. 111, p. 17–38, https://doi.org/10.1086/344663.

Yonkee, W.A., and Weil, A.B., 2015, Tectonic evolution of the Sevier and Laramide belts within the North American Cordillera orogenic system: Earth-Science Reviews, v. 150, p. 531–593, https://doi.org/10.1016/j.earscirev.2015.08.001.

Young, J.C., 1960, Structure and Stratigraphy in the North-Central Schell Creek Range, Eastern Nevada [Ph.D. dissertation]: Princeton, New Jersey, Princeton University, 207 p., 3 plates.

Zoback, M.L., Anderson, R.E., and Thompson, G.A., 1981, Cenozoic evolution of the state of stress and style of tectonism of the Basin and Range Province of the western United States: Philosophical Transactions of the Royal Society, v. 300, p. 407–434, https://doi.org/10.1098/rsta.1981.0073.

Zoback, M.L., McKee, E.H., Blakely, R.J., and Thompson, G.A., 1994, The northern Nevada rift: Regional tectonomagmatic relations and middle Miocene stress direction: Geological Society of America Bulletin, v. 106, p. 371–382, https://doi.org/10.1130/0016-7606(1994)106<0371:TNNRRT>2.3.CO;2.

Science Editor: David I. Schofield
Associate Editor: Bernhard Grasemann

Manuscript Received 20 November 2017
Revised Manuscript Received 26 May 2018
Manuscript Accepted 12 July 2018

Printed in the USA